Comparison of Micromixing Models for CFD Simulation of Nanoparticle Formation

Liguang Wang and Rodney O. Fox
Dept. of Chemical Engineering, Iowa State University, Ames, IA 50011

DOI 10.1002/aic.10173
Published online in Wiley InterScience (www.interscience.wiley.com).

Reactive precipitation is an important research topic in chemical engineering because of its numerous industrial applications in the formation of nanoparticles. Recently, computational fluid dynamics (CFD) has been successfully coupled with micromixing models and probability density function (PDF) methods to predict the effect of mixing on the particle size distribution. The micromixing model is generally based on the presumed PDF method. The objective of this work is to compare multienvironment-presumed PDFs and a recently proposed direct-quadrature-method-of-moments-interaction-by-exchange-with-the-mean (DQMOM-IEM) micromixing model with transported PDF predictions for the simulation of reactive precipitation, including simultaneous mixing-limited reaction, nucleation, and growth in a plug-flow reactor. DQMOM is applied to calculate the turbulent spurious dissipation rate for the multienvironment micromixing models. The results show that the DQMOM-IEM model agrees well with the transported PDF simulations, even when the number of nodes used in DQMOM is small (such as 2–4). Given the computational efficiency of the DQMOM-IEM model relative to transported PDF methods, this model offers great promise as a practical CFD tool for simulating plant-scale reactors. © 2004 American Institute of Chemical Engineers *AIChE J,* 50: 2217–2232, 2004
Keywords: micromixing, computational fluid dynamics (CFD), nanoparticle, reactive precipitation, probability density function (PDF) methods

Introduction

The unique chemical, electronic, magnetic, and optical properties of nanoscale particles have led to their evaluation and use in a broad range of industries, such as biotechnology, catalysis, data storage, energy storage, and microelectronics (Martin and Kohli, 2003; Roco, 1999, 2001; Söhnel and Garside, 1992; Tavare, 1995). Reactive precipitation, which involves mixing-limited reaction, nucleation, growth, and aggregation, is often of key importance in the processes that produce particles for these applications. The product properties, such as particle size distribution and morphology, result from micromixing and rapid reactive precipitation. When modeling these reactors using computational fluid dynamics (CFD), it is important to choose an appropriate micromixing model to efficiently and accurately simulate reactive precipitation.

The calculation of the chemical source term $\mathbf{S}(\boldsymbol{\phi})$ is one of the major issues when modeling turbulent reacting flows (Fox, 2003). The conventional closure for the chemical source term is to assume that the joint composition probability density function (PDF) can be represented by its moments. In general, this assumption has severe limitations and cannot predict complex competitive reactions (Fox, 2003). Another important approach works directly with the composition PDF. The joint composition PDF $f_{\boldsymbol{\phi}}$ of the scalars in a reacting flow is defined as

$$f_{\boldsymbol{\phi}}(\boldsymbol{\psi}; \mathbf{x}, t)d\boldsymbol{\psi} = P[\psi_\alpha < \phi_\alpha(\mathbf{x}, t) < \psi_\alpha + d\psi_\alpha, \alpha = \mathrm{A}, \mathrm{B}, \cdots] \tag{1}$$

where A, B, and so forth are the chemical "species" appearing in the reacting flow problem. For reactive precipitation, these

Correspondence concerning this article should be addressed to R.O. Fox at rofox@iastate.edu.

"species" can include the moments of the particle size distribution (Piton et al., 2000). The composition vector $\boldsymbol{\phi}$ has length N_s, as does its state-space counterpart $\boldsymbol{\psi}$. If $f_{\boldsymbol{\phi}}$ is known, the Reynolds-average chemical source term can be calculated exactly as follows

$$\langle \mathbf{S}(\boldsymbol{\phi}) \rangle = \int_0^{+\infty} \cdots \int_0^{+\infty} \mathbf{S}(\boldsymbol{\psi}) f_{\boldsymbol{\phi}}(\boldsymbol{\psi}; \mathbf{x}, t) d\boldsymbol{\psi} \tag{2}$$

In general, modeling approaches that attempt to find appropriate forms for $f_{\boldsymbol{\phi}}$ are known as PDF methods. PDF methods can be categorized as presumed and transported (Fox, 2003).

Several differences between the two types of models exist in terms of the discretization of the composition space, spatial transport, and the numerical scheme adopted. For example, the presumed form of the PDF in terms of a finite collection of delta functions may be inadequate for complex chemistry. For transported PDF methods, the shape of the joint scalar PDF is computed from its transport equation. However, transported PDF codes are generally much more CPU intensive than presumed PDF codes.

To solve the population balance equation (PBE), which is used to describe particulate flow phenomena, discretized population balance (DPB) methods (Hounslow et al., 1988; Lister et al., 1995) or the method of moments (MOM) (Leeuwen et al., 1996) can be applied. Previous results in different devices have shown that mixing plays an important role in the evolution of supersaturation and hence on nucleation and growth (Baldyga et al., 1995a; Fitchett and Tarbell, 1990; Marchisio et al., 2001a; Phillips et al., 1999). MOM is generally used in CFD because it requires only a few lower-order moments (usually ≤ 6) to describe the PBE. Several presumed PDF methods coupled with CFD have been used to study turbulent precipitation, including nucleation and growth, using MOM. A four-environment presumed PDF method has been used to investigate turbulent precipitation in a single-jet tubular reactor (Piton et al., 2000). Comparison between a three-environment presumed PDF and transported PDF methods for tubular flow precipitation has been made and some discrepancies were found in the predictions of m_0 and d_{43} in Marchisio et al. (2001b). Because transported PDF methods (Dopazo, 1994; Fox, 1996; Pope, 1985) are considered to be the state-of-the-art technique for solving micromixing and chemical reactions in turbulent flows, an important question to consider is whether multienvironment models can be constructed to yield equivalent results. This is the question to be answered in this work.

PDF Methods for Reactive Precipitation

A poorly micromixed, plug-flow reactor model (see Figure 1) will be used to compare the predictions of precipitation for different PDF methods (Wang and Fox, 2003). For this model, it is assumed that the turbulence fields (such as k and ε) are homogeneous and stationary. As shown in Figure 1, only $\langle U_z \rangle$ is nonzero and constant in the reactor. Further details on the model can be found in Wang and Fox (2003).

Transported PDF model

In transported PDF methods, the joint PDF is represented by a large number of "notional particles." The notional particles move in real and composition space by well-defined stochastic models (Pope, 1985). A detailed description of the PDF formulation and solution using Monte Carlo methods can be found in Fox (2003). Here we limit the discussion to the final transport equation of the joint composition PDF $f_{\boldsymbol{\phi}}(\boldsymbol{\psi}; x, t)$, made dimensionless by setting $t_z = z + \langle U_z \rangle t^*$, $t = t_z/(k/\varepsilon)$, and $x = \varepsilon y/(C_1 k^{1.5})$ [see Wang and Fox (2003) for details]

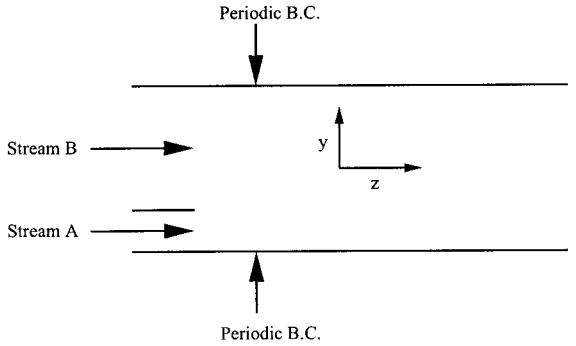

Figure 1. Poorly micromixed plug-flow reactor model.

$$\frac{\partial f_{\boldsymbol{\phi}}}{\partial t} = \Gamma_T \frac{\partial^2 f_{\boldsymbol{\phi}}}{\partial x^2} - \sum_{\alpha=1}^{N_s} \frac{\partial}{\partial \psi_\alpha} \left[\left(M_\alpha + \frac{k}{\varepsilon} S_\alpha(\boldsymbol{\psi}) \right) f_{\boldsymbol{\phi}} \right] \tag{3}$$

where $\Gamma_T = C_\mu/(Sc_T C_1^2) = 0.1286$ is the dimensionless turbulent diffusivity. Note that in Eq. 3 the source term $S_\alpha(\boldsymbol{\psi})$ appears in closed form.

In this work, we will use the IEM model to represent micromixing in the transported PDF simulations. The dimensionless IEM model can be written as

$$M_\alpha = \frac{C_\phi}{2} (\langle \phi_\alpha \rangle - \psi_\alpha) \tag{4}$$

where $C_\phi = 2$ is the nominal value of the mechanical-to-scalar time-scale ratio. The reader should keep in mind that many other transported PDF micromixing models are available in the literature (Fox, 2003). Thus, when comparing the transported PDF results with multienvironment PDF results it is imperative that the IEM model also be used in the multienvironment PDF model. As shown in Fox (2003), the problem of finding an equivalent multienvironment PDF model starting from a particular transported PDF micromixing model is relatively straightforward. However, the inverse problem of finding a transported PDF micromixing model from a particular multienvironment PDF model is still open. In this work, we will first compare results for the IEM model found by transported and multienvironment PDF methods. We will then show that consistent formulations of other multienvironment micromixing models are possible, and compare these results to the transported PDF results. The goal of these latter comparisons is to show that the choice of the micromixing model can have a strong effect on CFD predictions for reactive precipitation, and thus care must be taken to validate the models with simple inert-scalar mixing problems before they are used for reacting-scalar CFD.

Because of the high dimensionality of the state-space vector,

Table 1. Nonzero Initial Conditions for Notional Particles in the Transported PDF Model

	ξ	c_{A0}	c_{B0}
$0 \le x < 0.2$	1	100.0 mol/m^3	0
$0.2 \le x < 2$	0	0	11.1 mol/m^3

Eq. 3 cannot be solved directly using standard discretization methods. Instead, a Monte Carlo simulation is used with approximately 6000 notional particles [see Wang and Fox (2003) for details]. Every notional particle contains information concerning its position $\mathbf{X}$ and composition $\boldsymbol{\phi}$. The initial conditions for mixture fraction ξ, and reactant concentrations c_{A0} and c_{B0} are shown in Table 1. All other scalars are initially zero. The time step $\Delta t = 0.001$ is specified in the simulations. Spatial gradients in the x-direction are resolved using $n_{cell} = 100$ equally spaced grid cells in the periodic domain $x \in [0, 2]$. Thus, each grid cell contains approximately $n_p = 60$ notional particles, which can be used to generate a histogram estimate for $f_{\boldsymbol{\phi}}(\boldsymbol{\psi}; x, t)$ at fixed x and t (Fox, 2003). Alternately, the joint PDF can be visualized using scatter plots at fixed t using all (or a random subset) of the 6000 notional particles. This latter representation is particularly convenient when looking at conditional variables (such as reaction progress Y conditioned on mixture fraction ξ), and we will use it later to compare the different models. The multienvironment PDF simulations discussed below use the same mesh density and time step as the transported PDF simulations. Solutions have been compared for different mesh densities and time steps, and the parameters given above were found to be mesh independent. In the simulations, the calculations for turbulent diffusion and the chemical source terms are simply time split. During the source-term substep calculation, a stiff initial value ODE solver (Rosenbrock method) is used (Press et al., 1992). Alternatively, in situ adaptive tabulation (ISAT) can be used to efficiently evaluate the source terms, as described in Wang and Fox (2003).

Multienvironment PDF methods

In multienvironment PDF methods, the presumed composition PDF has the form

$$f_{\boldsymbol{\phi}}(\boldsymbol{\psi}; x, t) = \sum_{n=1}^{N_e} p_n(x, t) \prod_{\alpha=1}^{N_s} \delta[\psi_\alpha - \langle \phi_\alpha \rangle_n(x, t)] \qquad (5)$$

where N_e is the number of environments, p_n is the probability of environment n, and $\langle \boldsymbol{\phi} \rangle_n$ is the mean composition vector in environment n (Fox, 2003). For a 1-D inhomogeneous flow corresponding to Figure 1, the presumed PDF governing equations are as follows

$$\frac{\partial p_n}{\partial t} = \Gamma_T \frac{\partial^2 p_n}{\partial x^2} + \frac{k}{\varepsilon} \gamma G_n + a_n \qquad (6)$$

$$\frac{\partial \langle \mathbf{s} \rangle_n}{\partial t} = \Gamma_T \frac{\partial^2 \langle \mathbf{s} \rangle_n}{\partial x^2} + \frac{k}{\varepsilon} \gamma \mathbf{M}_n + p_n \frac{k}{\varepsilon} \mathbf{S}(\langle \boldsymbol{\phi} \rangle_n) + \mathbf{b}_n \qquad (7)$$

where $\langle \mathbf{s} \rangle_n = p_n \langle \boldsymbol{\phi} \rangle_n$ is the probability-weighted mean composition vector in environment n, γG_n is the rate of change of p_n attributed to micromixing, and $\gamma \mathbf{M}_n$ is the rate of change of $\langle \mathbf{s} \rangle_n$ attributed to micromixing. As discussed below, the choices of G_n and $\mathbf{M}_n$ are subject to constraints to conserve the sum of the probabilities and the mean compositions. However, many different consistent forms exist and result in different multienvironment micromixing models (Fox, 2003). As discussed below, the correction terms a_n and $\mathbf{b}_n$ are needed to ensure that the composition moments of order two and higher are correctly predicted in the presence of mean scalar gradients. Finally, $\mathbf{S}(\langle \boldsymbol{\phi} \rangle_n)$ is the (closed) source term evaluated at node composition $\langle \boldsymbol{\phi} \rangle_n$. Note that the extension of Eqs. 6 and 7 to 3-D inhomogeneous flows with turbulent convection is straightforward (Fox, 2003).

The specification of G_n and $\mathbf{M}_n$ depends on the definition of the micromixing model. Nonetheless, the conservation of probability requires that

$$\sum_{n=1}^{N_e} p_n = 1 \qquad (8)$$

and thus

$$\sum_{n=1}^{N_e} G_n = 0 \qquad (9)$$

The mean composition vector can be found from Eq. 5, and is given by

$$\langle \boldsymbol{\phi} \rangle = \sum_{n=1}^{N} p_n \langle \boldsymbol{\phi} \rangle_n = \sum_{n=1}^{N_e} \langle \mathbf{s} \rangle_n \qquad (10)$$

Because micromixing must leave the means unchanged (Fox, 2003), we require that

$$\sum_{n=1}^{N_e} \mathbf{M}_n = \mathbf{0} \qquad (11)$$

Similar constraints apply to the correction terms a_n and $\mathbf{b}_n$.

Summing Eq. 7 over n yields the transport equation for the mean compositions

$$\frac{\partial \langle \boldsymbol{\phi} \rangle}{\partial t} = \Gamma_T \frac{\partial^2 \langle \boldsymbol{\phi} \rangle}{\partial x^2} + \frac{k}{\varepsilon} \langle \mathbf{S}(\boldsymbol{\phi}) \rangle \qquad (12)$$

where the mean chemical source term is defined by

$$\langle \mathbf{S}(\boldsymbol{\phi}) \rangle = \sum_{n=1}^{N_e} p_n \mathbf{S}(\langle \boldsymbol{\phi} \rangle_n) \qquad (13)$$

The micromixing computations are performed at the subgrid level during the CFD calculation. Example expressions for γG_n and $\gamma \mathbf{M}_n$ for several different micromixing models (Fox,

Table 2. Two-Environment Model (2E)

Model Variable	$\gamma G_n,\ \gamma \mathbf{M}^{(n)}$	$a_n,\ \mathbf{b}_n$
p_1	$\gamma p_1 p_2$	$-\gamma_s p_1$
$\langle \mathbf{s} \rangle_1$	$\gamma p_1 \langle \mathbf{s} \rangle_2$	$-\gamma_s p_1 \langle \boldsymbol{\phi} \rangle_2$
$\langle \mathbf{s} \rangle_2$	$-\gamma p_1 \langle \mathbf{s} \rangle_2$	$\gamma_s p_1 \langle \boldsymbol{\phi} \rangle_2$

$p_2 = 1 - p_1,\ \langle \xi'^2 \rangle = p_1 p_2 \langle \xi \rangle_1^2,\ \langle \boldsymbol{\phi} \rangle_2 = \langle \mathbf{s} \rangle_2 / p_2$

$\gamma = \dfrac{\varepsilon_\xi}{\langle \xi'^2 \rangle}, \gamma_s = \dfrac{2}{\langle \xi \rangle_1^2} \Gamma_T \dfrac{\partial \langle \xi \rangle_1}{\partial x} \dfrac{\partial \langle \xi \rangle_1}{\partial x}$

2003) are listed in Tables 2–8. Consistent with the transported PDF simulations, the mixture-fraction variance dissipation rate ε_ξ is calculated by

$$\frac{k}{\varepsilon} \varepsilon_\xi = C_\phi \langle \xi'^2 \rangle \tag{14}$$

where $C_{\boldsymbol{\phi}} = 2$. The correction terms a_n and $\mathbf{b}_n$ are determined using the direct quadrature method of moments (DQMOM) (Marchisio and Fox, 2004), which will be described next.

Direct quadrature method of moments

DQMOM can be applied to derive the correction terms needed in Eqs. 6 and 7 (Marchisio and Fox, 2004). DQMOM begins with the joint composition PDF transport equation (Eq. 3). The derivation starts by inserting Eq. 5 into Eq. 3, and the following linear equation for the N_s scalars is found (Fox, 2003)

$$\sum_{n=1}^{N_e} \left[\left(1 - \sum_{\alpha=1}^{N_s} m_\alpha \right) \prod_{\alpha=1}^{N_s} \langle \phi_\alpha \rangle_n^{m_\alpha} \right] a_n + \sum_{n=1}^{N_e} \sum_{\alpha=1}^{N_s} \frac{\partial}{\partial \langle \phi_\alpha \rangle_n} \left(\prod_{\beta=1}^{N_s} \langle \phi_\beta \rangle_n^{m_\beta} \right) b_{\alpha n} = \sum_{n=1}^{N_e} \sum_{\alpha=1}^{N_s} \sum_{\beta=1}^{N_s} \frac{\partial^2}{\partial \langle \phi_\alpha \rangle_n \partial \langle \phi_\beta \rangle_n} \left(\prod_{\gamma=1}^{N_s} \langle \phi_\gamma \rangle_n^{m_\gamma} \right) p_n c_{\alpha\beta n} \tag{15}$$

where the right-hand side depends on the mean scalar gradients

Table 3. Three-Environment Model (3E)

Model Variable	$\gamma G_n,\ \gamma \mathbf{M}^{(n)}$	$a_n,\ \mathbf{b}_n$
p_1	$-\gamma p_1 (1 - p_1)$	$\gamma_{s1} p_3$
p_2	$-\gamma p_2 (1 - p_2)$	$\gamma_{s2} p_3$
$\langle \mathbf{s} \rangle_1$	$-\gamma (1 - p_1) \langle \mathbf{s} \rangle_1$	$\gamma_{s1} p_3 \langle \boldsymbol{\phi} \rangle_1$
$\langle \mathbf{s} \rangle_2$	$-\gamma (1 - p_2) \langle \mathbf{s} \rangle_2$	$\gamma_{s2} p_3 \langle \boldsymbol{\phi} \rangle_2$
$\langle \mathbf{s} \rangle_3$	$\gamma [(1 - p_1) \langle \mathbf{s} \rangle_1 + (1 - p_2) \langle \mathbf{s} \rangle_2]$	$-p_3 (\gamma_{s1} \langle \boldsymbol{\phi} \rangle_1 + \gamma_{s2} \langle \boldsymbol{\phi} \rangle_2)$

$p_3 = 1 - p_1 - p_2,\ \langle \boldsymbol{\phi} \rangle_n = \langle \mathbf{s} \rangle_n / p_n$ with $n = 1, 2$

$\gamma = \dfrac{\varepsilon_\xi}{p_1 (1 - p_1)(1 - \langle \xi \rangle_3)^2 + p_2 (1 - p_2) \langle \xi \rangle_3^2}$

$\gamma_{s1} = \dfrac{2 \langle \xi \rangle_3}{(1 - \langle \xi \rangle_3)^2} \Gamma_T \dfrac{\partial \langle \xi \rangle_3}{\partial x} \dfrac{\partial \langle \xi \rangle_3}{\partial x},\ \gamma_{s2} = \dfrac{2(1 - \langle \xi \rangle_3)}{\langle \xi \rangle_3^2} \Gamma_T \dfrac{\partial \langle \xi \rangle_3}{\partial x} \dfrac{\partial \langle \xi \rangle_3}{\partial x}$

$\langle \xi'^2 \rangle = p_1 (1 - p_1) - 2 p_1 p_3 \langle \xi \rangle_3 + p_3 (1 - p_3) \langle \xi \rangle_3^2$

Table 4. Four-Environment Model (4Ea)

Model Variable	$\gamma G_n,\ \gamma \mathbf{M}^{(n)}$	$a_n,\ \mathbf{b}_n$
p_1	$-\gamma p_1 (1 - p_1)$	0
p_2	$\gamma [p_1 (1 - p_1) - p_2 + p_3]$	0
p_3	$\gamma [p_2 - p_3 + p_4 (1 - p_4)]$	0
$\langle \mathbf{s} \rangle_1$	$-\gamma (1 - p_1) \langle \mathbf{s} \rangle_1$	0
$\langle \mathbf{s} \rangle_2$	$\gamma [(1 - p_1) \langle \mathbf{s} \rangle_1 - \langle \mathbf{s} \rangle_2 + \langle \mathbf{s} \rangle_3]$	$\mathbf{b}_2$
$\langle \mathbf{s} \rangle_3$	$\gamma [\langle \mathbf{s} \rangle_2 - \langle \mathbf{s} \rangle_3 + (1 - p_4) \langle \mathbf{s} \rangle_4]$	$\mathbf{b}_3$
$\langle \mathbf{s} \rangle_4$	$-\gamma (1 - p_4) \langle \mathbf{s} \rangle_4$	0

$p_4 = 1 - p_1 - p_2 - p_3,\ \langle \boldsymbol{\phi} \rangle_n = \langle \mathbf{s} \rangle_n / p_n$ with $n = 1, 4$

$\gamma = \dfrac{\varepsilon_\xi}{p_1 (1 - p_1)(1 - \langle \xi \rangle_2)^2 + (p_2 + p_3)(\langle \xi \rangle_2 - \langle \xi \rangle_3)^2 + p_4 (1 - p_4) \langle \xi \rangle_3^2}$

$\langle \xi'^2 \rangle = p_1 (1 - p_1) + p_2 (1 - p_2) \langle \xi \rangle_2^2 + p_3 (1 - p_3) \langle \xi \rangle_3^2 - 2 p_1 p_2 \langle \xi \rangle_2 - 2 p_1 p_3 \langle \xi \rangle_3 - 2 p_2 p_3 \langle \xi \rangle_2 \langle \xi \rangle_3$

$$c_{\alpha\beta n} \equiv \Gamma_T \frac{\partial \langle \phi_\alpha \rangle_n}{\partial x} \frac{\partial \langle \phi_\beta \rangle_n}{\partial x} \tag{16}$$

The $N_e(N_s + 1)$ unknowns $(a_n, b_{1n}, \ldots, b_{N_s n})$ are found by solving Eq. 15 with the same number of unique combinations of lower-order integer moments. The latter are specified by choosing unique sets of $(m_1, \ldots, m_{N_s})$ where $m_\alpha \in (0, 1, 2, \cdots)$. Note that in the absence of mean scalar gradients, $c_{\alpha\beta n} = 0$ and thus $a_n = 0$ and $\mathbf{b}_n = \mathbf{0}$ satisfy Eq. 15. Hence, as noted earlier, the correction terms are only needed in the presence of mean scalar gradients.

As an example of how a set of moments creates a linear equation, assume all $m_\alpha = 0$ in Eq. 15. It then follows that

$$\sum_{n=1}^{N_e} \left[\left(1 - \sum_{\alpha=1}^{N_s} m_\alpha \right) \prod_{\alpha=1}^{N_s} \langle \phi_\alpha \rangle_n^{m_\alpha} \right] a_n = a_1 + a_2 + \cdots + a_{N_e} \tag{17}$$

$$\sum_{n=1}^{N_e} \sum_{\alpha=1}^{N_s} \frac{\partial}{\partial \langle \phi_\alpha \rangle_n} \left(\prod_{\beta=1}^{N_s} \langle \phi_\beta \rangle_n^{m_\beta} \right) b_{\alpha n} = 0 \tag{18}$$

and

Table 5. Four-Environment Model (4Eb)

Model Variable	$\gamma G_n,\ \gamma \mathbf{M}^{(n)}$	$a_n,\ \mathbf{b}_n$
p_1	$-\gamma p_1 (1 - p_1)$	0
p_2	$\gamma p_1 (1 - p_1)$	0
p_3	$\gamma p_4 (1 - p_4)$	0
$\langle \mathbf{s} \rangle_1$	$-\gamma (1 - p_1) \langle \mathbf{s} \rangle_1$	0
$\langle \mathbf{s} \rangle_2$	$\gamma [(1 - p_1) \langle \mathbf{s} \rangle_1 - p_3 \langle \mathbf{s} \rangle_2 + p_2 \langle \mathbf{s} \rangle_3]$	$\mathbf{b}_2$
$\langle \mathbf{s} \rangle_3$	$\gamma [p_3 \langle \mathbf{s} \rangle_2 - p_2 \langle \mathbf{s} \rangle_3 + (1 - p_4) \langle \mathbf{s} \rangle_4]$	$\mathbf{b}_3$
$\langle \mathbf{s} \rangle_4$	$-\gamma (1 - p_4) \langle \mathbf{s} \rangle_4$	0

$p_4 = 1 - p_1 - p_2 - p_3,\ \langle \boldsymbol{\phi} \rangle_n = \langle \mathbf{s} \rangle_n / p_n$ with $n = 1, 4$

$\gamma = \dfrac{\varepsilon_\xi}{p_1 (1 - p_1)(1 - \langle \xi \rangle_2)^2 + 2 p_2 p_3 (\langle \xi \rangle_2 - \langle \xi \rangle_3)^2 + p_4 (1 - p_4) \langle \xi \rangle_3^2}$

$\langle \xi'^2 \rangle = p_1 (1 - p_1) + p_2 (1 - p_2) \langle \xi \rangle_2^2 + p_3 (1 - p_3) \langle \xi \rangle_3^2 - 2 p_1 p_2 \langle \xi \rangle_2 - 2 p_1 p_3 \langle \xi \rangle_3 - 2 p_2 p_3 \langle \xi \rangle_2 \langle \xi \rangle_3$

Table 6. DQMOM-IEM(2) Model

Model Variable	$\gamma G_n,\ \gamma \mathbf{M}^{(n)}$	$a_n,\ \mathbf{b}_n$
p_1	0	0
$\langle \mathbf{s} \rangle_1$	$\gamma(p_1\langle \mathbf{s} \rangle_2 - p_2\langle \mathbf{s} \rangle_1)$	$\mathbf{b}_1$
$\langle \mathbf{s} \rangle_2$	$\gamma(p_2\langle \mathbf{s} \rangle_1 - p_1\langle \mathbf{s} \rangle_2)$	$\mathbf{b}_2$

$p_2 = 1 - p_1$, $\langle \xi'^2 \rangle = p_1 p_2(\langle \xi \rangle_1 - \langle \xi \rangle_2)^2$, $\langle \boldsymbol{\phi} \rangle_n = \langle \mathbf{s} \rangle_n / p_n$ with $n = 1, 2$

$\gamma = \dfrac{\varepsilon_\xi}{2\langle \xi'^2 \rangle}$

$$\sum_{n=1}^{N_e} \sum_{\alpha=1}^{N_s} \sum_{\beta=1}^{N_s} \frac{\partial^2}{\partial \langle \phi_\alpha \rangle_n \partial \langle \phi_\beta \rangle_n} \left(\prod_{\gamma=1}^{N_s} \langle \phi_\gamma \rangle_n^{m_\gamma} \right) p_n c_{\alpha\beta n} = 0 \quad (19)$$

Thus, we obtain (as expected)

$$\sum_{n=1}^{N_e} a_n = 0 \quad (20)$$

As another example, consider the first-order moment where only $m_1 = 1$. Following the same steps as in Eqs. 17–19, we find

$$\sum_{n=1}^{N_e} b_{1n} = 0 \quad (21)$$

which indicates that the mean value of scalar 1 is conserved. The other first-order moments yield

$$\sum_{n=1}^{N_e} b_{\alpha n} = 0 \qquad \text{for } \alpha = 1, \ldots, N_s \quad (22)$$

Thus, DQMOM conserves both the probabilities and the scalar means as required.

The zero- and first-order moments must be satisfied in every case, and yield $N_s + 1$ linear equations. The remaining $(N_e - 1)(N_s + 1)$ linear equations must be found from higher-order moments. In general, depending on the value of N_e, second-order (either only one $m_\alpha = 2$ or two distinct $m_\alpha = 1$), and possibly third-order moments will be required to get a full-rank coefficient matrix $\mathbf{A}$ to solve the linear equation of the form

$$\mathbf{A}\boldsymbol{\alpha} = \mathbf{c} \quad (23)$$

where the vector of unknowns is defined by $\boldsymbol{\alpha} = [a_1, \ldots, a_{N_e}, b_{11}, b_{12}, \ldots, b_{N_s N_e}]^T$. Of course, $\mathbf{A}$ and $\mathbf{c}$ are found from Eq. 15. However, the user must find a linearly independent set of moments for which the rank of $\mathbf{A}$ is equal to $N_e(N_s + 1)$. Readers can find more information related to problems that can arise in choosing linearly independent moments in Marchisio and Fox (2004).

Table 7. DQMOM-IEM(3) Model

Model Variable	$\gamma G_n,\ \gamma \mathbf{M}^{(n)}$	$a_n,\ \mathbf{b}_n$
p_1	0	0
p_2	0	0
$\langle \mathbf{s} \rangle_1$	$\gamma(p_1(\langle \mathbf{s} \rangle_2 + \langle \mathbf{s} \rangle_3) - (1 - p_1)\langle \mathbf{s} \rangle_1)$	$\mathbf{b}_1$
$\langle \mathbf{s} \rangle_2$	$\gamma(p_2(\langle \mathbf{s} \rangle_1 + \langle \mathbf{s} \rangle_3) - (1 - p_2)\langle \mathbf{s} \rangle_2)$	$\mathbf{b}_2$
$\langle \mathbf{s} \rangle_3$	$\gamma(p_3(\langle \mathbf{s} \rangle_1 + \langle \mathbf{s} \rangle_2) - (1 - p_3)\langle \mathbf{s} \rangle_3)$	$\mathbf{b}_3$

$p_3 = 1 - p_1 - p_2$, $\langle \xi'^2 \rangle = \Sigma_{n=1}^3 p_n \langle \xi \rangle_n^2 - (\Sigma_{n=1}^3 p_n \langle \xi \rangle_n)^2$, $\langle \boldsymbol{\phi} \rangle_n = \langle \mathbf{s} \rangle_n / p_n$ with $n = 1, 3$

$\gamma = \dfrac{\varepsilon_\xi}{2\langle \xi'^2 \rangle}$

Table 8. DQMOM-IEM(4) Model

Model Variable	$\gamma G_n,\ \gamma \mathbf{M}^{(n)}$	$a_n,\ \mathbf{b}_n$
p_1	0	0
p_2	0	0
p_3	0	0
$\langle \mathbf{s} \rangle_1$	$\gamma(p_1(\langle \mathbf{s} \rangle_2 + \langle \mathbf{s} \rangle_3 + \langle \mathbf{s} \rangle_4) - (1 - p_1)\langle \mathbf{s} \rangle_1)$	$\mathbf{b}_1$
$\langle \mathbf{s} \rangle_2$	$\gamma(p_2(\langle \mathbf{s} \rangle_1 + \langle \mathbf{s} \rangle_3 + \langle \mathbf{s} \rangle_4) - (1 - p_2)\langle \mathbf{s} \rangle_2)$	$\mathbf{b}_2$
$\langle \mathbf{s} \rangle_3$	$\gamma(p_3(\langle \mathbf{s} \rangle_1 + \langle \mathbf{s} \rangle_2 + \langle \mathbf{s} \rangle_4) - (1 - p_3)\langle \mathbf{s} \rangle_3)$	$\mathbf{b}_3$
$\langle \mathbf{s} \rangle_4$	$\gamma(p_4(\langle \mathbf{s} \rangle_1 + \langle \mathbf{s} \rangle_2 + \langle \mathbf{s} \rangle_3) - (1 - p_4)\langle \mathbf{s} \rangle_4)$	$\mathbf{b}_4$

$p_4 = 1 - p_1 - p_2 - p_3$, $\langle \xi'^2 \rangle = \Sigma_{n=1}^4 p_n \langle \xi \rangle_n^2 - (\Sigma_{n=1}^4 p_n \langle \xi \rangle_n)^2$, $\langle \boldsymbol{\phi} \rangle_n = \langle \mathbf{s} \rangle_n / p_n$ with $n = 1, 4$

$\gamma = \dfrac{\varepsilon_\xi}{2\langle \xi'^2 \rangle}$

For the reactive precipitation case considered in this work, $N_s = 8$ and the scalars differ in value by several orders of magnitude (Wang and Fox, 2003). It should thus be noted that Eq. 15 is scalable, which means that we can scale $\langle \phi_\alpha \rangle$ by a factor C_α, and then use the scaled value to compute its gradient. After finding $b_{\alpha n}$ for the scaled variables, the correction term for the original scalar is simply equal to $C_\alpha b_{\alpha n}$. For reactive precipitation, this scaling scheme is extremely useful to avoid numerical errors in the linear solver needed to compute $\boldsymbol{\alpha}$ from Eq. 23. However, linearly dependent scalars will result in a singular covariance matrix, making the calculation unstable. Moreover, as reported in our earlier work (Marchisio and Fox, 2004), Eq. 15 does not ensure scalar boundedness. Another difficulty that occurs with certain multienvironment micromixing models (such as engulfment models) is that the composition $\langle \boldsymbol{\phi} \rangle_n$ is fixed, but p_n is allowed to change for particular values of n. Typically, the latter correspond to regions of "pure" or "unmixed" fluid (such as feed streams) in which no chemical reactions occur.

To overcome these difficulties, additional constraints must be added to DQMOM. To keep $\langle \boldsymbol{\phi} \rangle_n$ constant during micromixing, we must set $\mathbf{b}_n = a_n \langle \boldsymbol{\phi} \rangle_n$. To overcome the problems associated with boundedness, the following two constraints are required: (1) each scalar is treated independently (that is, no cross moments are used) and (2) $a_n = 0$ for all n. These two constraints result in the following simplified form of Eq. 15

$$\sum_{n=1}^{N_e} \langle \phi_\alpha \rangle_n^{m_\alpha - 1} b_{\alpha n} = (m_\alpha - 1) \sum_{n=1}^{N_e} \langle \phi_\alpha \rangle_n^{m_\alpha - 2} p_n c_{\alpha\alpha n}$$

$$\text{for } \alpha = 1, \ldots, N_s \quad (24)$$

Table 9. Initial Conditions for One-Environment Model (1E)

	p_1	$\langle\xi\rangle_1$
$0 \le x < 0.2$	1	1
$0.2 \le x < 2$	1	0

Table 10. Initial Conditions for Two-Environment Model

	p_1	p_2	$\langle\xi\rangle_1$	$\langle\xi\rangle_2$
$0 \le x < 0.2$	1	0	1	0
$0.2 \le x < 2$	0	1	1	0

where $m_\alpha = 1, 2, \ldots, N_e$. Thus, the correction terms $b_{\alpha n}$ for each scalar are found separately. When written in matrix form, the coefficient matrix on the left-hand side of Eq. 24 is a Vandermonde matrix, which often arises when reconstructing PDFs from their moments (Press et al., 1992). Although Vandermonde matrices are notoriously ill-conditioned for large N_e, this will not be a problem in applications of multienvironment PDF models because they are most attractive when N_e is small.

Note that by using Eq. 24, the first N_e moments of each scalar are forced to agree with the exact moments found from the joint PDF transport equation (that is, Eq. 3) in the *absence of chemical source terms.* When chemical source terms are present, the moment transport equation will not be closed, and thus the *exact* moments will be predicted only in the limit where N_e is very large. (Nevertheless, as shown later, excellent approximations for the moments can be found with small N_e.) Similar statements can be made concerning the Monte Carlo simulations in transported PDF methods where the number of notational particles per grid cell plays the same role as N_e. However, in Monte Carlo simulations of inert scalars the moments are in fact not predicted exactly because of statistical errors. Thus, because no statistical errors are present in the multienvironment models, they should yield superior predictions for inert scalar mixing as compared to transported PDF methods, especially in the limit of small N_e.

Multienvironment Micromixing Models

A number of different multienvironment micromixing models are proposed in Fox (2003). The correction terms used in these models were chosen to predict the correct mixture-fraction variance, and thus did not make use of DQMOM. Because these models are based on various mechanistic descriptions of micromixing (such as engulfment and deformation), it is of interest to determine what correction terms result from DQMOM. Note that in each of the models given below, the micromixing rate γ is chosen such that the mixture-fraction variance predictions for all of the models are the same as for the transported PDF simulations.

One-environment (1E)

In this model, complete micromixing is assumed at every grid point, and no correction terms are needed. We report this model here as a reference case for comparison against multienvironment PDF models that include micromixing. Table 9 reports the initial conditions for the 1E model (and hence of the initial mean compositions).

Two-environment (2E)

In this model, matter is transferred by engulfment only from environment 2 to environment 1. Hence $\langle\boldsymbol{\phi}\rangle_2$ is constant, and no reactions occur in environment 2. Because $\langle\boldsymbol{\phi}\rangle_2$ is forced to be constant, $\mathbf{b}_2 = a_2\langle\boldsymbol{\phi}\rangle_2$. Because $a_1 + a_2 = 0$ and $\mathbf{b}_1 + \mathbf{b}_2 = \mathbf{0}$, $a_1 = -a_2$ and $\mathbf{b}_1 = -\mathbf{b}_2 = -a_2\langle\boldsymbol{\phi}\rangle_2$. Thus, the only remaining unknown parameter is a_2. Because it is a scalar, we can choose only *one* of the second-order moments in DQMOM (such as $m_1 = 2$ in Eq. 15). Following Fox (2003), we choose to control the mixture-fraction variance and set the mixture fraction in environment 2 equal to zero. The resulting model variables are shown in Table 2 and initial conditions are given in Table 10.

Three-environment (3E)

In this model, environments 1 and 2 transfer matter by engulfment to environment 3 where reactions occur. Because $\langle\boldsymbol{\phi}\rangle_1$ and $\langle\boldsymbol{\phi}\rangle_2$ must remain constant, $\mathbf{b}_1 = a_1\langle\boldsymbol{\phi}\rangle_1$ and $\mathbf{b}_2 = a_2\langle\boldsymbol{\phi}\rangle_2$; hence $\mathbf{b}_3 = -a_1\langle\boldsymbol{\phi}\rangle_1 - a_2\langle\boldsymbol{\phi}\rangle_2$. Given that $a_3 = -a_1 - a_2$, DQMOM can be used to determine the *two* remaining unknowns: a_1 and a_2. Note that these are again scalar quantities, so we may choose at most two higher-order moments for use with Eq. 15. Consistent with the 2E model, we choose to control the second and third moments of the mixture fraction ($m_1 = 2$ and $m_1 = 3$ in Eq. 15). Following Fox (2003), we will let the mixture fraction be unity in environment 1 and zero in environment 2. Thus, spatial gradients in the mixture fraction are present only in environment 3. Letting $\alpha = 1$ denote the mixture fraction, we find $b_{11} = a_1$, $b_{12} = 0$, and $b_{13} = -a_1$. Using these values in Eq. 15 yields

$$(1 - \langle\xi\rangle_3)^2 a_1 + \langle\xi\rangle_3^2 a_2 = 2p_3c_{113} \qquad \text{for } m_1 = 2$$

$$(1 - 3\langle\xi\rangle_3^2 + 2\langle\xi\rangle_3^3)a_1 + 2\langle\xi\rangle_3^3 a_2 = 6\langle\xi\rangle_3 p_3 c_{113} \qquad \text{for } m_1 = 3 \quad (25)$$

which can be solved to find a_1 and a_2

$$a_1 = 2\,\frac{\langle\xi\rangle_3}{(1 - \langle\xi\rangle_3)^2}\,p_3c_{113} = \gamma_{s1}p_3$$

$$a_2 = 2\,\frac{(1 - \langle\xi\rangle_3)}{\langle\xi\rangle_3^2}\,p_3c_{113} = \gamma_{s2}p_3 \quad (26)$$

The resulting model variables are shown in Table 3, and initial conditions are given in Table 11.

Four-environment (4Ea and 4Eb)

In these models, environments 2 and 3 are formed by engulfment between environments 1 and 4. Reactions occur in environments 2 and 3. In model 4Ea, environments 2 and 3 exchange probability (see definitions of G_2 and G_3), whereas

Table 11. Initial Conditions for Three-Environment Model

	p_1	p_2	p_3	$\langle\xi\rangle_1$	$\langle\xi\rangle_2$	$\langle\xi\rangle_3$
$0 \le x < 0.2$	1	0	0	1	0	1/2
$0.2 \le x < 2$	0	1	0	1	0	1/2

Table 12. Initial Conditions for Four-Environment Models

	p_1	p_2	p_3	p_4	$\langle\xi\rangle_1$	$\langle\xi\rangle_2$	$\langle\xi\rangle_3$	$\langle\xi\rangle_4$
$0 \le x < 0.2$	1	0	0	0	1	1	0	0
$0.2 \le x < 2$	0	0	0	1	1	1	0	0

in model 4Eb they do not. Note that the forms of correction terms will be the same for both models. Given that $\langle\boldsymbol{\phi}\rangle_1$ and $\langle\boldsymbol{\phi}\rangle_4$ must remain constant, $\mathbf{b}_1 = a_1\langle\boldsymbol{\phi}\rangle_1$ and $\mathbf{b}_4 = a_4\langle\boldsymbol{\phi}\rangle_4$; hence $\mathbf{b}_2 + \mathbf{b}_3 = -a_1\langle\boldsymbol{\phi}\rangle_1 - a_4\langle\boldsymbol{\phi}\rangle_4$. For this case, the compositions in environments 2 and 3 are free to move according to the combined effects of micromixing, the source terms, and the correction terms. To ensure boundedness for the scalars, we will invoke the constraint $a_n = 0$ for all n, and use Eq. 24 with $m_\alpha = 1$ and 2 to find $b_{\alpha 2}$ and $b_{\alpha 3}$. This process yields

$$b_{\alpha 2} = \frac{p_2 c_{\alpha\alpha 2} + p_3 c_{\alpha\alpha 3}}{\langle\phi_\alpha\rangle_2 - \langle\phi_\alpha\rangle_3} = -b_{\alpha 3} \tag{27}$$

Note that although this is a four-environment model and one would expect to be able to control moments up to order four using DQMOM, because two environments have fixed compositions we can control the moments only up to order two. The resulting model variables are shown in Tables 4 and 5 and initial conditions are given in Table 12.

As an example of the multienvironment PDF model equations, consider the 4Eb model shown in Figure 2. The micromixing and correction terms in Table 5 yield the following equations

$$\frac{\partial p_1}{\partial t} = \Gamma_T \frac{\partial^2 p_1}{\partial x^2} - \frac{k}{\varepsilon}\gamma p_1(1 - p_1)$$

$$\frac{\partial p_2}{\partial t} = \Gamma_T \frac{\partial^2 p_2}{\partial x^2} + \frac{k}{\varepsilon}\gamma p_1(1 - p_1)$$

$$\frac{\partial p_3}{\partial t} = \Gamma_T \frac{\partial^2 p_3}{\partial x^2} + \frac{k}{\varepsilon}\gamma p_4(1 - p_4) \tag{28}$$

$$\frac{\partial\langle\mathbf{s}\rangle_1}{\partial t} = \Gamma_T \frac{\partial^2\langle\mathbf{s}\rangle_1}{\partial x^2} - \frac{k}{\varepsilon}\gamma(1 - p_1)\langle\mathbf{s}\rangle_1$$

$$\frac{\partial\langle\mathbf{s}\rangle_2}{\partial t} = \Gamma_T \frac{\partial^2\langle\mathbf{s}\rangle_2}{\partial x^2} + \frac{k}{\varepsilon}\gamma[(1 - p_1)\langle\mathbf{s}\rangle_1 - p_3\langle\mathbf{s}\rangle_2 + p_2\langle\mathbf{s}\rangle_3] + \mathbf{b}_2 + p_2\frac{k}{\varepsilon}\mathbf{S}(\langle\boldsymbol{\phi}\rangle_2)$$

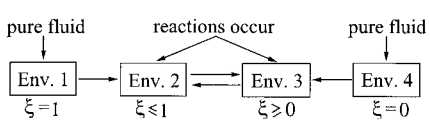

Figure 2. In the four-environment model (4Eb), environment 1 initially contains unmixed fluid with ξ = 1 and environment 4 contains unmixed fluid with ξ = 0.

Precipitation reactions occur in environments 2 and 3 when $0 < \xi < 1$.

$$\frac{\partial\langle\mathbf{s}\rangle_3}{\partial t} = \Gamma_T \frac{\partial^2\langle\mathbf{s}\rangle_3}{\partial x^2} + \frac{k}{\varepsilon}\gamma[p_3\langle\mathbf{s}\rangle_2 - p_2\langle\mathbf{s}\rangle_3 + (1 - p_4)\langle\mathbf{s}\rangle_4] + \mathbf{b}_3 + p_3\frac{k}{\varepsilon}\mathbf{S}(\langle\boldsymbol{\phi}\rangle_3)$$

$$\frac{\partial\langle\mathbf{s}\rangle_4}{\partial t} = \Gamma_T \frac{\partial^2\langle\mathbf{s}\rangle_4}{\partial x^2} - \frac{k}{\varepsilon}\gamma(1 - p_4)\langle\mathbf{s}\rangle_4 \tag{29}$$

where the relation $p_4 = 1 - p_1 - p_2 - p_3$ is used to eliminate the equation for p_4.

DQMOM-IEM(N_e) Micromixing Model

In all of the multienvironment PDF models discussed above, the concentrations of the scalars in some of the environments remain unchanged throughout the micromixing process, which requires that the correction terms calculated by DQMOM be treated differently. These multienvironment PDF models were originally constructed by invoking different micromixing mechanisms (such as engulfment and deformation). However, these mechanisms are not consistent with the IEM model that is used in the transported PDF simulations. Therefore, differences between the results found with the multienvironment PDF and the transported PDF methods are to be expected for arbitrary values of N_e. Hence, to make quantitative comparisons between the two methods, it is necessary to introduce the DQMOM-IEM(N_e) micromixing model. As shown in Fox (2003), the forms of the exchange terms in the DQMOM-IEM micromixing model are particularly simple

$$G_n = 0 \qquad \text{and} \qquad \mathbf{M}_n = p_n(\langle\boldsymbol{\phi}\rangle - \langle\boldsymbol{\phi}\rangle_n) \tag{30}$$

The definition of $\langle\boldsymbol{\phi}\rangle$ in terms of $\langle\mathbf{s}\rangle_n$ (Eq. 10) can be used to reexpress the micromixing model in terms of p_n and $\langle\mathbf{s}\rangle_n$ (see Tables 6–8). The correction terms $\mathbf{b}_n$ are found directly from Eq. 24. In theory, because the micromixing models are exactly the same, as N_e increases the predictions from the DQMOM-IEM(N_e) micromixing model should exactly approach those from the transported PDF model (Eq. 3). We will investigate the rate of convergence of the two methods later.

When applying the DQMOM-IEM(N_e) micromixing model to inhomogeneous flows, we have found that because $G_n = a_n = 0$ the initial/boundary conditions for p_n cannot be everywhere null. Indeed, for the mixing problem under consideration, if $p_n(x, 0) = 0$ then $p_n(x, t)$ will remain null for all t. To overcome this difficulty, we have found that it suffices to initialize $p_n(x, t)$ such that it is nonzero (such as unity) on some subdomain in $x \in [0, 2]$. The corresponding weighted scalars $\langle\mathbf{s}\rangle_n$ can then be chosen to yield the desired initial scalar distribution. However, specifying that $p_n(x, 0)$ be nonzero does not uniquely determine its value. For example, in Table 13 two sets of initial conditions are shown that yield the same initial moments. In the first set, $p_n(x, 0)$ varies with x and the initial mixture fractions $\langle\xi\rangle_n(x, 0)$ are constant for each n. In the second set, p_n is constant and $\langle\xi\rangle_n(x, 0)$ is allowed to vary with x. As shown in the Appendix, the second choice leads to unrealizable solutions for which $\langle\xi\rangle_n(x, t)$ lies outside of the interval [0, 1] for certain values of x. In general, we have found

Table 13. Two Sets of Initial Conditions for DQMOM-IEM(2) Model

	p_1	p_2	$\langle\xi\rangle_1$	$\langle\xi\rangle_2$
$0 \le x < 0.2$	1	0	1	0
$0.2 \le x < 2$	0	1	1	0
$0 \le x < 0.2$	1/2	1/2	1	1
$0.2 \le x < 2$	1/2	1/2	0	0

that unrealizable solutions occur only when $\langle\xi\rangle_n(x, 0)$ is allowed to vary with x. Thus, in addition to satisfying $p_n(x, 0) > 0$ on a subdomain in x, we must also require that $\langle\xi\rangle_n(x, 0)$ be constant for each n. Note that for $N_e > 2$, these conditions do not uniquely determine $p_n(x, 0)$ and $\langle\xi\rangle_n(x, 0)$. Thus, to investigate how the choice of initial conditions affects the model predictions, we will use the two sets of initial conditions reported in Table 14 ($N_e = 3$) and Table 15 ($N_e = 4$).

DQMOM-IEM(2)

In this two-environment micromixing model, environments 1 and 2 exchange matter with each other; hence, reactions occur in both environments (see Fig. 3). Model variables are shown in Table 6, and two sets of initial conditions are given in Table 11. (Recall that the second set is unrealizable, as mentioned above.) Applying Eq. 24, the correction terms for $\langle s_\alpha\rangle$ are found to be

$$b_{\alpha 1} = \frac{p_1 c_{\alpha\alpha 1} + p_2 c_{\alpha\alpha 2}}{\langle\phi_\alpha\rangle_1 - \langle\phi_\alpha\rangle_2} = -b_{\alpha 2} \tag{31}$$

Note that $b_{\alpha 1}$ is not defined when $\langle\phi_\alpha\rangle_1 = \langle\phi_\alpha\rangle_2$ (that is, when the compositions in the two nodes coincide). In our simulations, we find that this occurs only on isolated points in the x-domain. To overcome this difficulty, whenever it occurs we simply compute $\mathbf{b}_n$ using the average of the two neighboring grid points in the x-domain. Another approach is to use the perturbation method discussed in the Appendix.

DQMOM-IEM(3)

For this three-environment micromixing model, the model variables are shown in Table 7 and two sets of initial conditions are given in Table 14. In the first set, the longer region ($0.2 \le x < 2$, $\xi = 0$) is represented by two environments with $p_2 = 3/4$, $\langle\xi\rangle_2 = 0$ and $p_3 = 1/4$, $\langle\xi\rangle_3 = 0$ when $0.2 \le x < 2$. In the second set, the longer region is represented by two environments with $p_2 = p_3 = 1/2$. Like the DQMOM-IEM(2) micromixing model, the correction terms are obtained by applying Eq. 24 for each scalar. Note that with $N_e = 3$, the correction terms will ensure that the first three moments of the mixture fraction are identical for all realizable sets of initial conditions. However, differences in the moments of order four and higher are expected.

Table 14. Two Sets of Initial Conditions for DQMOM-IEM(3) Model

	p_1	p_2	p_3	$\langle\xi\rangle_1$	$\langle\xi\rangle_2$	$\langle\xi\rangle_3$
$0 \le x < 0.2$	1	0	0	1	0	0
$0.2 \le x < 2$	0	3/4	1/4	1	0	0
$0 \le x < 0.2$	1	0	0	1	0	0
$0.2 \le x < 2$	0	1/2	1/2	1	0	0

Table 15. Two Sets of Initial Conditions for DQMOM-IEM(4) Model

	p_1	p_2	p_3	p_4	$\langle\xi\rangle_1$	$\langle\xi\rangle_2$	$\langle\xi\rangle_3$	$\langle\xi\rangle_4$
$0 \le x < 0.2$	3/4	1/4	0	0	1	1	0	0
$0.2 \le x < 1.1$	0	0	1	0	1	1	0	0
$1.1 \le x < 2$	0	0	0	1	1	1	0	0
$0 \le x < 0.2$	1/2	1/2	0	0	1	1	0	0
$0.2 \le x < 2$	0	0	1/2	1/2	1	1	0	0

DQMOM-IEM(4)

For this four-environment micromixing model, model variables are shown in Table 8 and two sets of initial conditions are given in Table 15. In the first set, the shorter region ($0 \le x < 0.2$) is represented by two environments with $p_1 = 3/4$, $\langle\xi\rangle_1 = 1$ and $p_2 = 1/4$, $\langle\xi\rangle_2 = 1$ when $0 \le x < 0.2$. On the other hand, the longer region ($0.2 \le x < 2.0$) is split into two equal regions where $p_3 = 1$, $\langle\xi\rangle_3 = 0$ when $0.2 \le x < 1.1$; and $p_4 = 1$, $\langle\xi\rangle_4 = 0$ when $1.1 \le x < 2$. In the second set, both regions are represented by two environments with $p_n = 1/2$. Note that other possible sets of initial conditions exist (the longer region could be represented by $p_2 = p_3 = p_4 = 1/3$) and lead to realizable solutions. Similar to the DQMOM-IEM(2) micromixing model, the correction terms are found by applying Eq. 24 for each scalar. Note that with $N_e = 4$, the correction terms will ensure that the first four moments of the mixture fraction are identical for all realizable sets of initial conditions. However, differences in the moments of order five and higher are expected.

As an explicit example of the transport equations, consider the DQMOM-IEM(2) micromixing model. In this case, the relation $p_2 = 1 - p_1$ can be used to eliminate the equation for p_2. The transport equations can then be manipulated to yield

$$\frac{\partial p_1}{\partial t} = \Gamma_T \frac{\partial^2 p_1}{\partial x^2} \tag{32}$$

$$\frac{\partial\langle\mathbf{s}\rangle_1}{\partial t} = \Gamma_T \frac{\partial^2\langle\mathbf{s}\rangle_1}{\partial x^2} + \frac{k}{\varepsilon}\gamma(p_1\langle\mathbf{s}\rangle_2 - p_2\langle\mathbf{s}\rangle_1) + \mathbf{b}_1 + p_1\frac{k}{\varepsilon}\mathbf{S}(\langle\boldsymbol{\phi}\rangle_1) \tag{33}$$

and

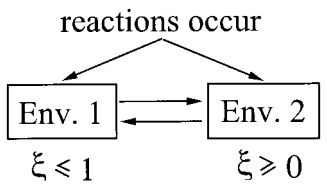

Figure 3. In the DQMOM-IEM(2) model, environment 1 initially contains unmixed fluid with $\xi = 1$ and environment 2 contains unmixed fluid with $\xi = 0$.

Precipitation reactions occur in environments 1 and 2 when $0 < \xi < 1$.

Table 16. Composition Variables and Source Terms

ϕ_1	$S_1(\boldsymbol{\phi})$	ξ	0
ϕ_2	$S_2(\boldsymbol{\phi})$	Y	$\frac{\rho k_v}{M\xi_s c_{A0}} 3G(\xi, Y)m_2$
ϕ_3	$S_3(\boldsymbol{\phi})$	m_0	$B(\xi, Y)$
ϕ_4	$S_4(\boldsymbol{\phi})$	m_1	$G(\xi, Y)m_0$
ϕ_5	$S_5(\boldsymbol{\phi})$	m_2	$2G(\xi, Y)m_1$
ϕ_6	$S_6(\boldsymbol{\phi})$	m_3	$3G(\xi, Y)m_2$
ϕ_7	$S_7(\boldsymbol{\phi})$	m_4	$4G(\xi, Y)m_3$

$$\frac{\partial\langle \mathbf{s}\rangle_2}{\partial t} = \Gamma_T \frac{\partial^2\langle \mathbf{s}\rangle_2}{\partial x^2} + \frac{k}{\varepsilon}\gamma(p_2\langle \mathbf{s}\rangle_1 - p_1\langle \mathbf{s}\rangle_2) + \mathbf{b}_2 + p_2\frac{k}{\varepsilon}\mathbf{S}(\langle\boldsymbol{\phi}\rangle_2) \tag{34}$$

where $\mathbf{b}_1$ and $\mathbf{b}_2$ are determined by DQMOM (that is, Eq. 31).

Reactive-Precipitation Source Terms

As previously mentioned, MOM can be applied to solve the PBE for simultaneous nucleation and growth (Randolph and Larson, 1988). The dimensionless Reynolds-averaged transport equation for the moments of the particle size distribution can be written as

$$\frac{\partial\langle m_j\rangle}{\partial t} = \Gamma_T \frac{\partial^2\langle m_j\rangle}{\partial x^2} + 0^j\frac{k}{\varepsilon}\langle B\rangle + j\frac{k}{\varepsilon}\langle G m_{j-1}\rangle \tag{35}$$

where B is the nucleation rate and G is the crystal growth rate. The first five moments are of particular interest because they are related to the total particle number density (m_0), the total particle surface area ($k_a m_2$), the total solids volume ($k_v m_3$), and the mean particle size ($d_{43} = m_4/m_3$), where k_a is surface shape factor and k_v is volume shape factor. In general, both shape factors depend on crystal morphology. Note that the nonlinear terms in Eq. 35 for nucleation and growth are not closed. These terms are strongly affected by micromixing (Piton et al., 2000), which can be modeled using PDF methods (such as transported or multienvironment PDF models).

Using MOM and a multienvironment micromixing model, a set of seven composition variables must be used for each environment, resulting in a composition vector of the form $\boldsymbol{\phi} = [\xi, Y, m_0, \ldots, m_4]^T$. In addition to the mixture fraction and moments, Y is the reaction-progress variable defined below. In Table 16, the source terms that are used for each scalar are reported. These source terms are used in Eqs. 3 and 7 to account for reactive precipitation. In this study, barium sulfate precipitation kinetics are used ($A = Ba^{2+}$ and $B = SO_4^{2-}$) with nonpremixed inlet concentrations of $c_{A0} = 100.0$ mol/m^3 and $c_{B0} = 11.1$ mol/m^3, unless stated otherwise. The other model constants needed to define the source term for Y are $\rho = 4500$ kg/m^3, $k_v = 5$, and $M = 0.224$ kg/mol.

The nucleation [$B(\xi, Y)$] and growth [$G(\xi, Y)$] rates appearing in Table 16 can be calculated by using the reactant concentrations for a one-step, nonpremixed reaction

$$A + B \rightarrow C$$

The local species concentrations are related to local mixture fraction ξ and reaction-progress variable Y by the following expressions (Marchisio et al., 2001a)

$$c_A = c_{A0}(\xi - \xi_s Y) \tag{36}$$

$$c_B = c_{B0}[1 - \xi - (1 - \xi_s)Y] \tag{37}$$

where $\xi_s = c_{B0}/(c_{A0} + c_{B0})$. In the inflow streams, the reaction-progress variable is null ($Y = 0$) and the mixture fraction is either $\xi = 0$ or $\xi = 1$. Thus, c_{A0} and c_{B0} are just the species concentrations in the inflow streams. As shown below, the nucleation and growth rates depend on the supersaturation, which is a function of c_A and c_B, and hence of ξ and Y. Based on the initial conditions, $\xi_s = \langle\xi\rangle = 0.1$; hence, Y will approach unity when reactant B is depleted.

The nucleation rate used in this study is obtained from Baldyga et al. (1995b):

- When $\Delta c \leq 10$ mol/m^3, *heterogeneous* nucleation occurs

$$B(\xi, Y) = 2.83 \times 10^{10}(\Delta c)^{1.775} \qquad [1/(\text{m}^3\ \text{s})] \tag{38}$$

When $\Delta c > 10$ mol/m^3, *homogeneous* nucleation occurs:

$$B(\xi, Y) = 2.53 \times 10^{-3}(\Delta c)^{15} \qquad [1/(\text{m}^3\ \text{s})] \tag{39}$$

where the supersaturation is defined by $\Delta c = (c_A c_B)^{1/2} - k_s^{1/2}$ [mol/m^3], and the solubility product of barium sulfate is $k_s = 1.14 \times 10^{-4}$ mol^2/m^6 at room temperature.

The growth kinetics (Baldyga et al., 1995b) are described by a two-step diffusion–adsorption model (Nielsen and Toft, 1984)

$$G(\xi, Y) = k_r(\Delta c_s)^2 = k_d(c_A - c_{As}) = k_d(c_B - c_{Bs}) \qquad [\text{m/s}] \tag{40}$$

where $\Delta c_s = (c_{As}c_{Bs})^{1/2} - k_s^{1/2}$ [mol/m^3], $k_r = 5.8 \times 10^{-8}$ (m/s)(m^6/mol^2) (Nielsen, 1984), and k_d is the mass transfer coefficient. $c_{\alpha s}$ is the concentration of species α near the surface of the crystal at the limit of the adsorption layer. According to Nagata (1975), k_d is size-dependent but remains nearly constant for particles smaller than 10 μm. As a consequence, k_d should fall in the range between 10^{-7} and 10^{-8} (m/s)(m^3/mol) (Baldyga et al., 1995b). [More discussion on mass transfer to microparticles can be found in Armentante and Kirwan (1989).] In this work, k_d is fixed to be 10^{-7} (m/s)(m^3/mol). Other expressions for the nucleation and growth kinetics of barium sulfate can be found in Aoun et al. (1996, 1999), Wei and Garside (1997), Schwarzer and Peukert (2002), and Jones (2002). For example, more complex expressions are required to predict accurately the effect of nonstoichiometric conditions on the reactive precipitation process, and activity coefficients should be introduced for high feed concentrations (Baldyga and Orciuch, 2001). However, the qualitative predictions of all available kinetics expressions are similar, as is their sensitivity to micromixing. Thus, the conclusions drawn in this work concerning (for example) the agreement between the trans-

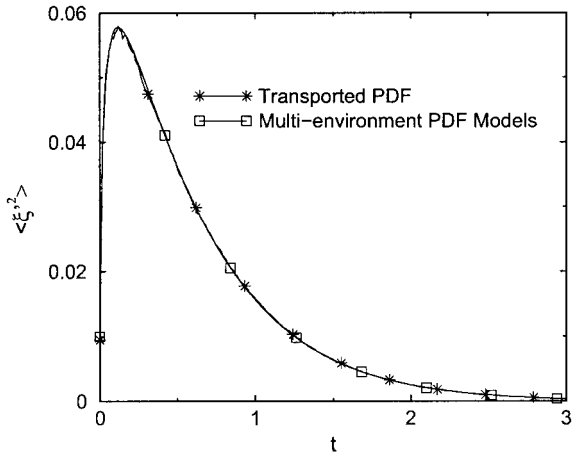

Figure 4. Evolution of the mixture-fraction variance $\langle \xi'^2 \rangle$ for multienvironment and transported PDF models.

ported PDF and the DQMOM-IEM models should apply to all kinetic models used for reactive precipitation of barium sulfate. On the other hand, agglomeration processes can be an important step in the evolution of particle size. The quadrature method of moments can be used to simulate this process (Marchisio et al., 2004; Wang and Fox, 2003).

Results and Discussion

Mixture-fraction moments

Because they can be written in closed form, it is useful first to compare the mixture-fraction moments predicted by the various models. Because ξ is an inert scalar, its spatial mean value $[\langle \xi \rangle(x, t)]$ depends only on the initial conditions $\langle \xi \rangle(x, 0)$ (which is the same for all models) and turbulent diffusivity

$$\frac{\partial \langle \xi \rangle}{\partial t} = \Gamma_T \frac{\partial^2 \langle \xi \rangle}{\partial x^2} \tag{41}$$

Thus, as expected, all of the multienvironment PDF models exactly reproduce the solution to this expression. On the other hand, the transported PDF model predicts a statistically equivalent solution that approaches the exact solution as the number of particles increases. Consistent with statistical sampling theory, the statistical error scales like $n_p^{-1/2}$.

By construction, for all of the micromixing models ($N_e \geq 2$) the mixture-fraction variance ($\langle \xi'^2 \rangle$) is governed by

$$\frac{\partial \langle \xi'^2 \rangle}{\partial t} = \Gamma_T \frac{\partial^2 \langle \xi'^2 \rangle}{\partial x^2} + 2\Gamma_T \left(\frac{\partial \langle \xi \rangle}{\partial x} \right)^2 - 2\langle \xi'^2 \rangle \tag{42}$$

with initial condition $\langle \xi'^2 \rangle(x, 0) = 0$. (For $N_e = 1$, the variance is null for all t.) Thus, because of the gradient in the mixture-fraction mean, variance is produced in the reactor and then decays for large t. In Figure 4, the x-average mixture-fraction variances calculated using the various PDF models are presented. Note that all reported variables including $\langle \xi'^2 \rangle$, m_0, d_{43}, B, and Y are averaged across the x-axis in this work to generate line plots. Nevertheless, surface plots of $\langle \xi'^2 \rangle(x, t)$ were also compared and found to agree for the various models. As expected, $\langle \xi'^2 \rangle$ calculated from different multienvironment PDF models are all identical and very close to the (statistically noisy) transported PDF result. Spatial contour plots of $\langle \xi \rangle$ and $\langle \xi'^2 \rangle$ calculated from the multienvironment and transported PDF models were also found to agree. Finally, results for $\langle \xi \rangle$ and $\langle \xi'^2 \rangle$ found with different initial conditions for the DQMOM-IEM micromixing models were identical.

As we mentioned previously, the DQMOM correction terms ensure that the first N_e moments ($1, 2, \ldots, N_e$) are exactly the same in the transported PDF and the DQMOM-IEM(N_e) models. For example, in the DQMOM-IEM(3) model, $\langle \xi \rangle$, $\langle \xi^2 \rangle$, and $\langle \xi^3 \rangle$ are exactly the same as in the transported PDF model. The expression to calculate the *central* moments of the mixture fraction using the multienvironment PDF model is

$$\langle \xi'^m \rangle = \langle (\xi - \langle \xi \rangle)^m \rangle = \sum_{n=1}^{N_e} p_n (\langle \xi \rangle_n - \langle \xi \rangle)^m \tag{43}$$

Note that because the multienvironment PDF models do not involve random processes, the moments found from Eq. 43 will be free of statistical error. On the other hand, in the transported PDF method, it is straightforward to obtain the cell values of $\langle \xi^m \rangle$ and $\langle \xi'^m \rangle$ using ensemble averages. However, these estimates are subject to statistical error, and for large m the number of notional particles must often be increased to control this error. For $m \geq 3$, the standardized central moments are defined by

$$\mu_m = \frac{\langle \xi'^m \rangle}{\langle \xi'^2 \rangle^{m/2}} \tag{44}$$

where the Gaussian values are $\mu_3 = 0$, $\mu_4 = 3$, $\mu_5 = 0$, and $\mu_6 = 15$. Recall that the mixture-fraction PDF in a turbulent flow is known to approach a Gaussian PDF for large t (Eswaran and Pope, 1988). However, it is also well known that the IEM model does not generate a Gaussian PDF in a scalar mixing layer (Tsai and Fox, 1998), which is quite similar to the reactor geometry used in this work.

In Figure 5, μ_3 and μ_4 for the DQMOM-IEM(N_e) models are plotted together with the results from the transported PDF model. To control the statistical error in the central moments, it was necessary to use 500 notional particles per grid cell in the transported PDF model. Given that the mean composition fields can be adequately estimated with 60 notional particles, the use of 500 particles requires a nearly tenfold increase in the computational cost. As noted above, the IEM model does not produce long-time Gaussian statistics for this flow. However, as expected, the mixture-fraction moments of order N_e and smaller found from the DQMOM-IEM(N_e) model agree well with the transported PDF model. Note that the same cannot necessarily be said for all moments. For example, noninteger moments, or integer moments of order $N_e + 1$ and higher, are not constrained to follow the exact solution. Nevertheless, as shown in Figure 6, μ_5 and μ_6 found from DQMOM-IEM(N_e) with $N_e \leq 4$ are also in good agreement with the transported PDF model (at a fraction of the computational cost!).

By construction, the mixture-fraction moments of the DQMOM-IEM model closely follow the transported PDF

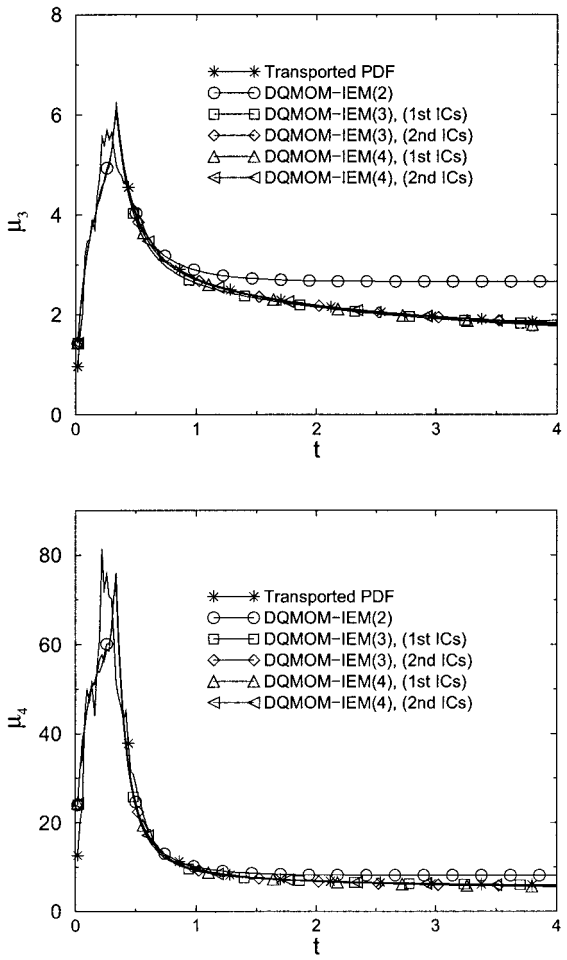

Figure 5. Evolution of the third and fourth standardized central moments of the mixture fraction for the DQMOM-IEM and transported PDF models.

Top: Third standardized central moment μ_3. Bottom: Fourth standardized central moment μ_4. Note that the results from both ICs in DQMOM-IEM(3) and (4) are plotted.

model. (Recall that both use the IEM model to close the micromixing term.) In contrast, the multienvironment models presented earlier do not use the IEM model and hence it can be expected that the central moments predicted by these models will differ from the transported PDF model. As shown in Figure 7, the third and fourth standardized central moments for the various models are quite different from the transported PDF results. In general, the 2E model predicts smaller central moments than the other models, and the results for the 3E and 4E models are very similar. Although none of these models approaches the Gaussian limit for large times, the reader should appreciate the fact that it should be possible to use alternative definitions for G_n and $\mathbf{M}^{(n)}$ that generate Gaussian statistics in the lower-order central moments. Obviously, the number of moments that can be controlled is limited by N_e. For example, with $N_e = 3$ it should be possible to define a multienvironment micromixing model for which μ_3 approaches zero. This flexibility in choosing the micromixing functions can be contrasted with transported PDF methods for which the development of micromixing models is much more difficult (Fox, 2003).

Based on the results presented for the mixture fraction, we can conclude that the DQMOM-IEM model yields a surprisingly accurate representation of inert scalar mixing, even for small N_e at a fraction of the computational cost of the transported PDF model. However, for the multienvironment PDF models to be useful for reactive precipitation, the same must be true for reacting scalars. We will examine this subject next by applying the models to reactive precipitation of barium sulfate.

Predictions for reactive precipitation

In Figures 8–10, the evolution of $\langle Y \rangle$, $\langle m_0 \rangle$, and $\langle d_{43} \rangle$ averaged across the x-axis are presented for a characteristic mixing time of $k/\varepsilon = 1$ s. From these figures, we can immediately draw the conclusion that, because the curves are significantly different for each model, reactive precipation under these feed conditions is sensitive to micromixing. Next, we can note that the DQMOM-IEM(N_e) results are very close to the transported PDF results for all values of N_e. Indeed, the results for different N_e all fall onto nearly the same curve. On the other hand, the predictions of the 1E and 2E models are far from those of the transported PDF simulation. As a general rule, as the number of environments increases (that is, 3E and 4E), the predictions become closer to the transported PDF results. Recall that only for the 4E models did the DQMOM correction

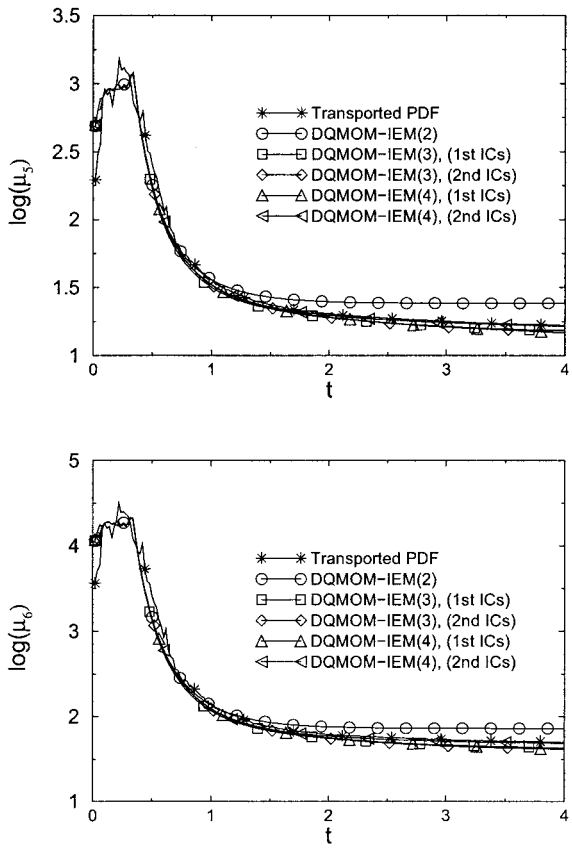

Figure 6. Evolution of the fifth and sixth standardized central moments of the mixture fraction for the DQMOM-IEM and transported PDF models.

Top: Fifth standardized central moment μ_5. Bottom: Sixth standardized central moment μ_6. Note that the results from both ICs in DQMOM-IEM(3) and (4) are plotted.

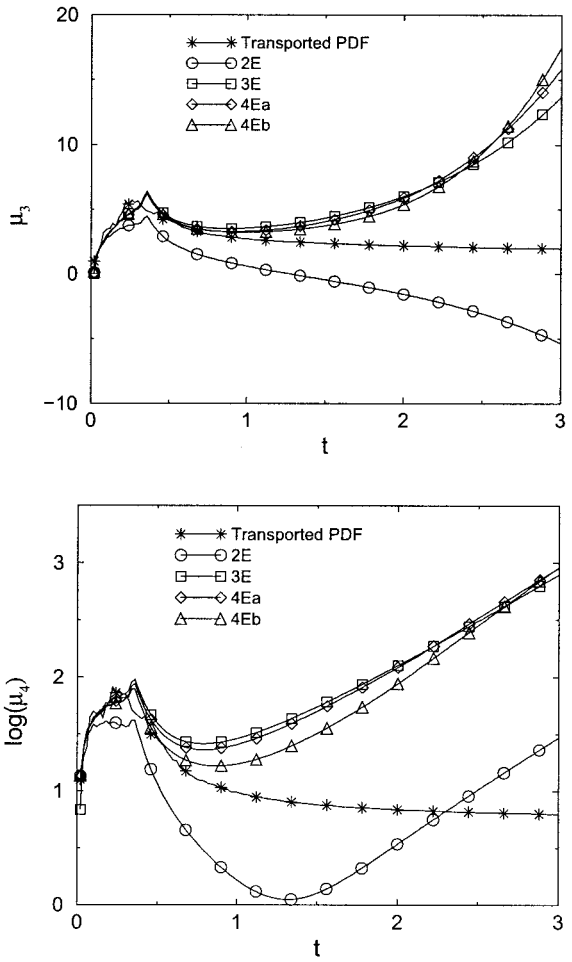

Figure 7. Evolution of the third and fourth standardized central moments of the mixture fraction for the multienvironment micromixing models.

Top: Third standardized central moment μ_3. Bottom: Fourth standardized central moment μ_4.

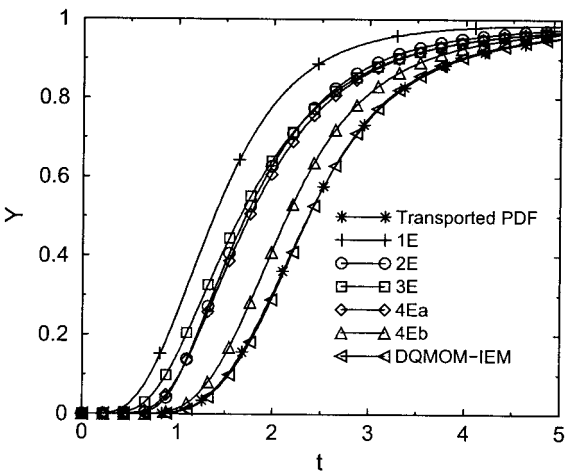

Figure 8. Evolution of the mean reaction-process variable $\langle Y \rangle$ for the multienvironment and transported PDF models.

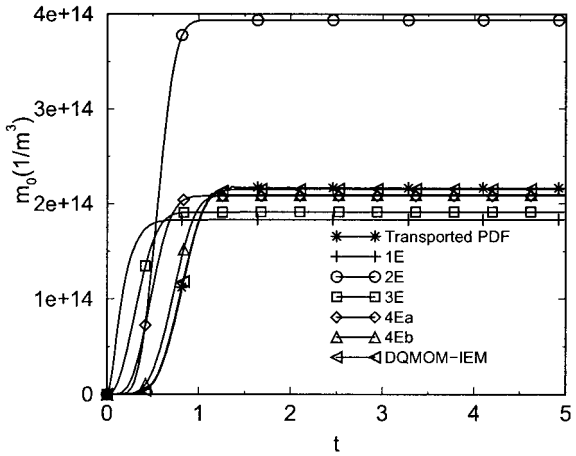

Figure 9. Evolution of mean particle number density $\langle m_0 \rangle$ for the multienvironment and transported PDF models.

terms control the second-order moments of the reacting scalars (see Tables 4 and 5). Also, because of its formulation, it can be noted that the 4Eb model reduces to the DQMOM-IEM(2) model in the limit where $p_1 = p_4 = 0$. It is thus not surprising that the 4Eb model results are closest to the transported PDF results in Figures 8–10.

The convergence of the DQMOM-IEM(N_e) models toward the transported PDF model for increasing N_e can be investigated by defining the relative error for each scalar

$$\varepsilon_\alpha = \frac{1}{K} \sum_{k=1}^{K} \frac{|\langle \phi_\alpha \rangle^{\mathrm{DQMOM}}(k\Delta t) - \langle \phi_\alpha \rangle^{\mathrm{PDF}}(k\Delta t)|}{\langle \phi_\alpha \rangle^{\mathrm{PDF}}(k\Delta t)} \tag{45}$$

where $\langle \phi_\alpha \rangle^{\mathrm{DQMOM}}(k\Delta t)$ is the average value across the x-axis on the kth time step using the DQMOM-IEM model, and $\langle \phi_\alpha \rangle^{\mathrm{PDF}}(k\Delta t)$ is the corresponding average found using the transported PDF model (that is, the curves shown in Figures 8–10). Note that for the mixture fraction ($\alpha = 1$), this error

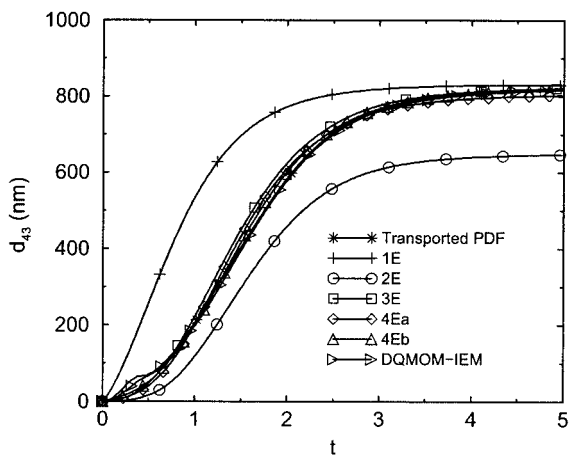

Figure 10. Evolution of mean particle size $\langle d_{43} \rangle$ for the multienvironment and transported PDF models.

Table 17. Relative Error for Different DQMOM-IEM Models

ε_α, %	ξ	Y	m_0	m_1	m_2	m_3	m_4
DQMOM-IEM(2)	0.25	8.71	1.96	3.27	5.61	8.71	12.4
DQMOM-IEM(3)	0.26	4.91	1.10	2.15	3.56	4.91	6.30
DQMOM-IEM(4)	0.26	3.78	0.61	1.22	2.82	3.78	5.23

would be zero if there were no statistical or numerical errors (such as because of grid spacing and number of notional particles used in transported PDF simulations). In Table 17, the relative errors are shown for $N_e = 2$–4. It is obvious that when more environments are used in the DQMOM-IEM model, smaller relative errors are found. Observing the source terms for Y and m_3 in Table 16, we see that they differ only by a constant, which explains why Y and m_3 have the same relative error. As is obvious from Figures 8–10, the relative errors reported in Table 17 are much smaller than the relative error between the multienvironment and the transported PDF models. Hence, there is little incentive to try to decrease the relative error by using larger values of N_e before making comparisons with experimental data to determine which micromixing model performs the best.

Although the DQMOM-IEM models predict similar results for reactive precipitation, we should comment that the predictions might be more sensitive to N_e for other cases. However, it should still hold that using more environments will result in more accurate results. On the other hand, as previously stated, N_e should be kept relatively small so that the Vandermonde matrix resulting from Eq. 24 does not become ill-conditioned, leading to numerical difficulties.

Homogeneous nucleation determines the characteristics of the precipitation near the inlet of the reactor (see Figure 11). In Figures 8 and 9, we can observe that the highest rate of increase in $\langle Y \rangle$ happens after the highest rate of increase in $\langle m_0 \rangle$. Homogeneous nucleation produces a large number of particles and thus the supersaturated species can find a large solid surface area for growth. From the modeling perspective, when m_0 increase significantly, a large value of m_2 (crystal surface area) is expected. Correspondingly, the source term for Y

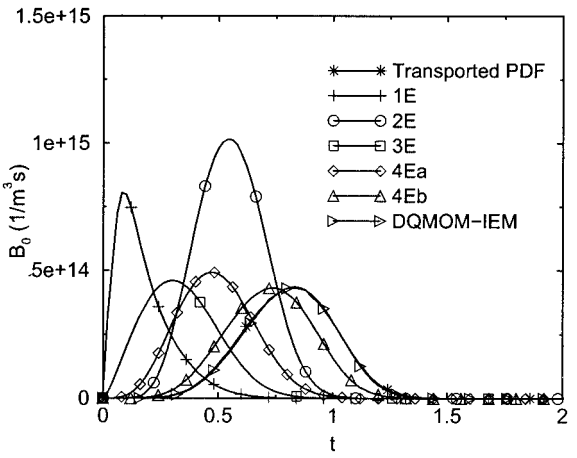

Figure 11. Evolution of mean nucleation rate $\langle B \rangle$ for the multienvironment and transported PDF models.

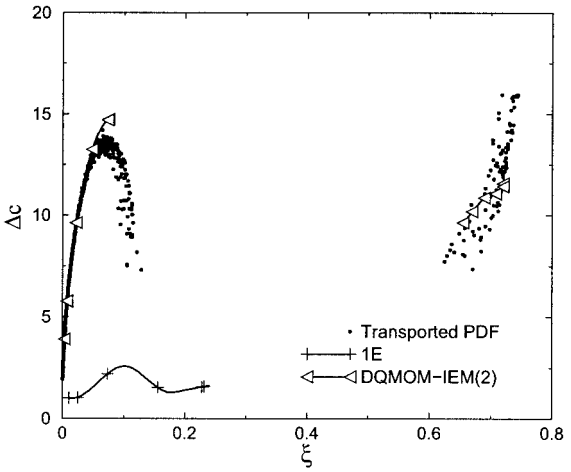

Figure 12. Scatter plot of supersaturation Δc conditioned on the mixture fraction ξ at $t = 0.5$ for the 1E, DQMOM-IEM(2), and transported PDF models (high concentrations).

becomes large (see Table 16), which means that appreciable species consumption occurs in the reactor. For different models, predictions of the mean nucleation rate $\langle B \rangle$ are different (see Figure 11). Depending on the presumed shape of the joint PDF, the mixture fractions in the environments are different for different multienvironment PDF models, although their mean mixture fraction and mixture-fraction variance are identical. For example, with the 2E model the peak mean nucleation rate is significantly higher than that of the other models. This is mainly attributed to the fact that the "engulfing" environment stays in the homogeneous nucleation regime for a longer period than that seen for the other models. In general, we can conclude that the value of the mixture fraction in an environment largely determines the degree of supersaturation, and thus the nucleation and growth rates near the inlet. The choice of the micromixing model can thus have a strong effect on the predictions. As noted above, the choice of the micromixing model can be made only by comparison with carefully designed reactive-precipitation experiments using a canonical turbulent flow (such as homogeneous turbulence).

To explore the question of why the results for the DQMOM-IEM models are so close to the transported PDF model, we present scatter plots (see Figures 12–14) of m_0, Y, and Δc conditioned on the value of mixture fraction ξ at a representative dimensionless time of $t = 0.5$ (scatter plots for other times are similar to $t = 0.5$) for high inlet concentrations of $c_A = 200.0$ mol/m^3, $c_B = 22.2$ mol/m^3. The higher concentrations are used to enhance the homogeneous nucleation rate, and thereby make the system more sensitive to micromixing. In these figures, predictions from the 1E, DQMOM-IEM(2), and transported PDF models are shown. Note that the scatter plots are constructed by random sampling of particles across the x-axis for fixed t. Thus, for the 1E model there is one "particle" per node; for the 2E model there are two; and for the transported PDF model there are $n_p = 60$. It is obvious that the DQMOM-IEM(2) model predicts scatter plots very similar to those from the transported PDF model; hence, the predictions for reactive precipitation from these two models are close. The

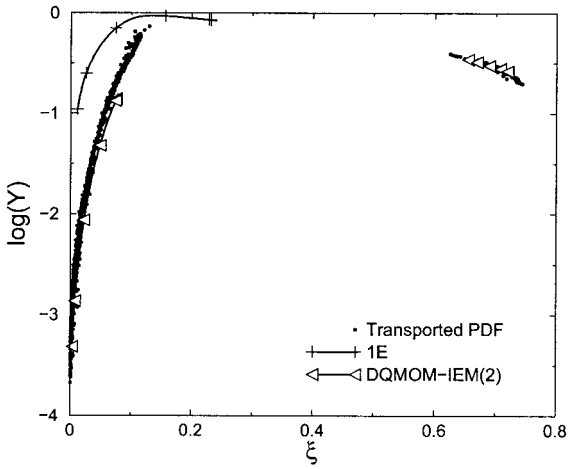

Figure 13. Scatter plot of reaction-progress variable Y conditioned on the mixture fraction ξ at t = 0.5 for the 1E, DQMOM-IEM(2), and transported PDF models (high concentrations).

only obvious difference between the DQMOM-IEM(2) and transported PDF results is that the latter has more scatter around the conditional mean. In fact, the DQMOM-IEM(2) model appears to correspond roughly to the mixture-fraction conditional mean $\langle \boldsymbol{\phi} | \xi \rangle$. As more environments are added [such as DQMOM-IEM(3)], the DQMOM-IEM model will develop scatter about the conditional mean and gradually approach the transported PDF result for large N_e. In contrast, the predictions of the 1E model are poor compared with those of the transported PDF, which means that a micromixing model is needed to simulate this reaction. We also compared other conditional plots for variables such as m_2 and growth rate (G) at different times, and so forth, and the results are analogous to those shown in Figures 12–14.

Cases with different mixing times (k/ε = 0.2, 0.5, 1.5 s), lower concentrations (c_A = 80.0 mol/m^3, c_B = 8.9 mol/m^3), excess species (Case 1: c_A = 200.0 mol/m^3, c_B = 11.1 mol/m^3; Case 2: c_A = 100.0 mol/m^3, c_B = 22.2 mol/m^3; Case 3: c_A = 10.0 mol/m^3, c_B = 111.1 mol/m^3) were also tested. For all of these cases, it was found that the predictions of the DQMOM-IEM model closely match the results from the transported PDF model. We can thus conclude that the DQMOM-IEM model yields an equivalent representation of reacting scalar mixing for reactive precipitation, even for small N_e. The conclusion that the DQMOM-IEM(N_e) models yield results very close to the transported PDF model is remarkable given the fact that the multienvironment PDF models take a completely different simulation approach from the transported PDF model, resulting in a considerable difference in CPU time. For example with reactive precipitation, a transported PDF simulation with n_p = 60 required approximately 408 min, whereas the DQMOM-IEM(2) model required approximately 13 min on a SunFire 6800 (900 MHz) for the same time step on an identical mesh. Moreover, because the multienvironment micromixing models are formulated in an Eulerian frame, they can be easily integrated into existing finite-volume CFD codes. We should note here that some commercial CFD codes run much more slowly if spatial gradients are used for the micromixing, but this is a numerical algorithm problem that must be addressed by commercial CFD code developers. On the other hand, the computation of complex chemistry can be very expensive and cause instability. As shown elsewhere, the in situ adaptive tabulation (ISAT) algorithm can be used as a solution to source term instability and to speed up the computation (Wang and Fox, 2003). The multienvironment micromixing models should thus be ideally suited for CFD simulations of nanoparticle formation by reactive precipitation in plant-scale chemical reactors.

Conclusions

CFD simulation of turbulent reactive precipitation of barium sulfate with nucleation and growth in a poorly micromixed plug-flow reactor was investigated in this work. The predictions of multienvironment and transported PDF models are compared. For the first time, DQMOM is formulated and applied to approximate the composition PDF transport equation. When properly chosen, the resulting DQMOM correction terms enforce agreement between selected lower-order moments of the mixture-fraction PDF and the exact moment transport equations. Likewise, for reacting scalars, the multienvironment PDF model provides a closure for the chemical source term, and the DQMOM correction terms enforce the correct behavior of the lower-order moments under the influence of turbulent diffusivity. Results for reactive precipitation show that the DQMOM-IEM model agrees closely with a transported PDF model in which the IEM model has been used to close the molecular mixing term. Because the multienvironment PDF model is much less computationally intensive than the transported PDF model, it is easy and extremely promising to couple the simple Eulerian-based multienvironment PDF models with a commercial CFD code for realistic industrial problems. Future work in turbulent reactive precipitation should focus on obtaining detailed experimental data in homogeneous turbulence that can be used to determine which multienvironment micromixing model provide the best description of reactive precipitation.

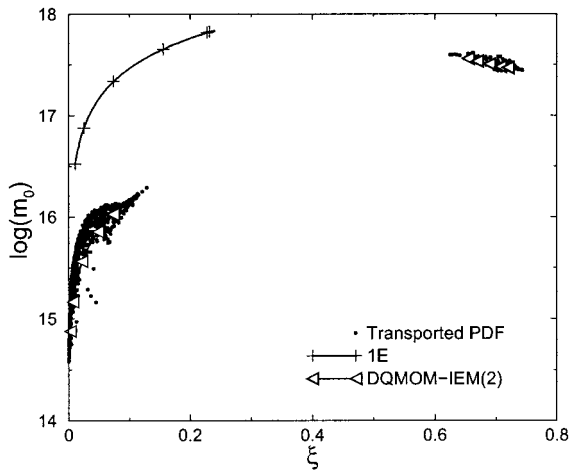

Figure 14. Scatter plot of particle number density m_0 conditioned on the mixture fraction ξ at t = 0.5 for the 1E, DQMOM-IEM(2), and transported PDF models (high concentrations).

Acknowledgment

This work was financially supported by the National Science Foundation (CTS-9985678) and the U.S. Department of Energy (DE-FC07-01ID14087).

Literature Cited

Aoun, M., E. Plasari, R. David, and J. Villermaux, "Are Barium Sulphate Kinetics Sufficiently Known for Testing Precipitation Reactor Models," *Chem. Eng. Sci.,* **51**, 2449 (1996).

Aoun, M., E. Plasari, R. David, and J. Villermaux, "A Simultaneous Determination of Nucleation and Growth Rates from Batch Spontaneous Precipitation," *Chem. Eng. Sci.,* **54**, 1161 (1999).

Armentante, P. M., and D. J. Kirwan, "Mass Transfer to Microparticles in Agitated System," *Chem. Eng. Sci.,* **44**, 2781 (1989).

Baldyga, J., and W. Orciuch, "Barium Sulphate Precipitation in a Pipe—An Experimental Study and CFD Modeling," *Chem. Eng. Sci.,* **56**, 2435 (2001).

Baldyga, J., W. Podgorska, and H. Phohrechy, "Mixing Precipitation Model with Application to Double Feed Semibatch Precipitation," *Chem. Eng. Sci.,* **50**, 1281 (1995a).

Baldyga, J., W. Podgorska, and R. Pohorechi, "Mixing-Precipitation Model with Application to Double Feed Semibatch Precipitation," *Chem. Eng. Sci.,* **50**, 1281 (1995b).

Dopazo, C., "Recent Developments in PDF Methods," *Turbulent Reacting Flows,* P. A. Libby and F. A. Williams, eds., Academic Press, New York, 375 (1994).

Eswaran, V., and S. B. Pope, "Direct Numerical Simulations of the Turbulent Mixing of a Passive Scalar," *Phys. Fluids,* **31**, 506 (1988).

Fitchett, D. E., and J. M. Tarbell, "Effect of Mixing on the Precipitation of Barium Sulfate in an MSMPR Reactor," *AIChE J.,* **36**, 511 (1990).

Fox, R. O., "The Fokker–Plank Closure for Turbulent Molecular Mixing: Passive Scalars," *Phys. Fluids A,* **4**, 1230 (1996).

Fox, R. O., *Computational Models for Turbulent Reacting Flows,* Cambridge University Press, Cambridge, UK (2003).

Hounslow, M. J., R. L. Ryall, and V. R. Marshall, "A Discretized Population Balance for Nucleation, Growth, and Aggregation," *AIChE J.,* **34**, 1821 (1988).

Jones, C. M., "Using Discrete Distributions to Analyze CSD Data from MSMPR Crystallizers," *AIChE J.,* **48**, 1448 (2002).

Leeuwen, M. L. V., O. S. L. Bruinsma, and G. M. V. Rosmalen, "Influence of Mixing on the Product Quality in Precipitation," *Chem. Eng. Sci.,* **51**, 2595 (1996).

Lister, J. D., D. J. Smit, and M. J. Hounslow, "Adjustable Discretized Population Balance for Growth and Aggregation," *AIChE J.,* **41**, 591 (1995).

Marchisio, D. L., A. A. Barresi, and R. O. Fox, "Simulation of Turbulent Precipitation in a Semi-Batch Taylor–Couette Reactor Using Computational Fluid Dynamics," *AIChE J.,* **47**, 664 (2001a).

Marchisio, D. L., and R. O. Fox, "Direct Quadrature Method of Moments: Derivation, Analysis and Applications," *Aerosol Sci. and Technol.,* submitted (2004).

Marchisio, D. L., R. O. Fox, A. A. Barresi, and G. Baldi, "On the Comparison between Presumed and Full PDF Methods for Turbulent Precipitation," *Ind. Eng. Chem. Res.,* **40**, 5132 (2001b).

Marchisio, D. L., J. T. Pikturna, R. O. Fox, R. D. Vigil, and A. A. Barresi, "Quadrature Method of Moments for Population Balances with Nucleation, Growth, and Aggregation," *AIChE J.,* **49**, 1266 (2003).

Martin, C. R., and P. Kohli, "The Emerging Field of Nanotube Biotechnology," *Nature,* **2**, 29 (2003).

Nagata, S., *Mixing. Principles and Applications,* Kodansha, Tokyo, Japan (1975).

Nielsen, A. E., "Electrolyte Crystal Growth Mechanisms," *J. Cryst. Growth,* **67**, 289 (1984).

Nielsen, A. E., and J. M. Toft, "Electrolyte Crystal Growth Kinetics," *J. Cryst. Growth,* **67**, 278 (1984).

Phillips, R., S. Rohani, and J. Baldyga, "Micromixing in a Single Feed Semi-Batch Precipitation Process," *AIChE J.,* **45**, 82 (1999).

Piton, D., R. O. Fox, and B. Marcant, "Simulation of Fine Particle Formation by Precipitation Using Computational Fluid Dynamics," *Can. J. Chem. Eng.,* **78**, 983 (2000).

Pope, S. B., "PDF Methods for Turbulent Reacting Flows," *Prog. Energy Combust. Sci.,* **11**, 119 (1985).

Press, W. H., S. A. Teukolsky, W. T. Vetterling, and B. P. Flannery, *Numerical Recipes in Fortran 77,* Cambridge University Press, Cambridge, UK (1992).

Randolph, A. D., and M. A. Larson, *Theory of Particulate Process,* 2nd Edition, Academic Press, San Diego (1988).

Roco, M. C., "Nanoparticles and Nanotechnology Research," *J. Nanoparticle Res.,* **1**, 1 (1999).

Roco, M. C., "International Strategy for Nanotechnology Research and Development," *J. Nanoparticle Res.,* **3**, 353 (2001).

Schwarzer, H. C., and W. Peukert, "Nanoparticle Precipitation: Experimental Investigation, Modeling and Process Simulation," Proc. of 15th International Symposium on Industrial Crystallization, Sorrento, Italy (2002).

Söhnel, O., and J. Garside, *Precipitation: Basic Principles and Industrial Applications,* Butterworth–Heinemann, Oxford, UK (1992).

Tavare, N. S., *Industrial Crystallization: Process Simulation Analysis and Design,* Plenum, New York (1995).

Tsai, K., and R. O. Fox, "The BMC/GIEM Model for Micromixing in Non-Premixed Turbulent Reacting Flows," *Ind. Eng. Chem. Res.,* **37**, 2131 (1998).

Wang, L., and R. O. Fox, "Application of In-Situ Adaptive Tabulation to CFD Simulation of Nano-Particle Formation by Reactive Precipitation," *Chem. Eng. Sci.,* **58**, 4387 (2003).

Wei, H., and J. Garside, "Application of CFD Modelling to Precipitation Systems," *Trans. IChemE, Chem. Eng. Res. Des.,* **75**(Part A), 219 (1997).

Appendix

This appendix is to illustrate how the choice of the initial conditions affects the boundedness of the mixture fraction, and how the initial singularity in the Vandermonde matrix (Eq. 24) is handled in the numerical implementation. As an example of initial conditions (ICs) that lead to unrealizable results, we will use the second set in Table 13 for DQMOM-IEM(2). Moreover, because micromixing makes the problem less severe, the analysis is done with $\gamma = 0$. Hence, only turbulent diffusion and the DQMOM correction terms are considered. The corresponding governing equations are shown in Eqs. 33 and 34. A simple explicit central-difference scheme can be used to solve the set of ODEs for $\langle \mathbf{s} \rangle_k$:

$$\langle s \rangle_{k,i}^{t+\Delta t} = \langle s \rangle_{k,i}^{t} + \frac{\Gamma_T}{\Delta x^2} \left(\langle s \rangle_{k,i+1}^{t} - 2\langle s \rangle_{k,i}^{t} + \langle s \rangle_{k,i-1}^{t} \right) \Delta t + (-1)^k \frac{p_1 c_{\xi\xi 1,i}^{t} + p_2 c_{\xi\xi 2,i}^{t}}{\langle \xi \rangle_{2,i}^{t} - \langle \xi \rangle_{1,i}^{t}} \Delta t \qquad \text{for } k = 1, 2 \quad \text{(A1)}$$

where $\langle s \rangle_{k,i}^{t+\Delta t}$ is the updated value of $\langle s \rangle_k (= p_k \langle \xi \rangle_k)$ at grid i and time $t + \Delta t$, Δx is the (constant) grid spacing, and Δt is the time step.

The first issue that must be addressed is the fact that $\langle \xi \rangle_1$ and $\langle \xi \rangle_2$ have the same initial conditions and governing transport equations, and thus will have the same value at every grid point. Hence, the final term on the right-hand side of Eq. A1 is singular, and a perturbation method must be used to separate $\langle \xi \rangle_1$ and $\langle \xi \rangle_2$ for $0 < t$. In general, any set of initial conditions with zero scalar variance will lead to a singular Vandermonde matrix in DQMOM-IEM. To make the Vandermonde matrix nonsingular, the following perturbation is used:

$$\langle \xi \rangle_{k,i}^{t} = \langle \xi \rangle_{k,i}^{t} - (-1)^k \varepsilon \quad \text{(A2)}$$

where ε is a small positive number. As noted in the main text, for ICs where $\langle \boldsymbol{\phi} \rangle_k$ is constant for each k, this perturbation suffices to generate well-behaved realizable concentration vec-

tors for all environments n. However, as shown below, a boundedness problem arises for initial conditions wherein $\langle\xi\rangle_k$ depends of x at $t = 0$ (such as the second ICs in Table 13).

For the second ICs in Table 13, we have $p_1 = p_2 = 0.5$ for all t. Therefore, by dividing Eq. A1 by p_k, we obtain

$$\langle\xi\rangle_{k,i}^{t+\Delta t} = \langle\xi\rangle_{k,i}^{t} + \frac{\Gamma_T}{\Delta x^2}\left(\langle\xi\rangle_{k,i+1}^{t} - 2\langle\xi\rangle_{k,i}^{t} + \langle\xi\rangle_{k,i-1}^{t}\right)\Delta t + (-1)^k \frac{c_{\xi\xi1,i}^{t} + c_{\xi\xi2,i}^{t}}{\langle\xi\rangle_{2,i}^{t} - \langle\xi\rangle_{1,i}^{t}}\Delta t \quad \text{(A3)}$$

The explicit, central-difference scheme to compute $c_{\xi\xi k,i}$ is

$$c_{\xi\xi k,i}^{t} = \frac{\Gamma_T}{4\Delta x^2}\left(\langle\xi\rangle_{k,i+1}^{t} - \langle\xi\rangle_{k,i-1}^{t}\right)^2 \qquad \text{for } k = 1, 2 \quad \text{(A4)}$$

The initial conditions require that $\langle\xi\rangle_{k,i}^{0}$ be either 0 or 1, and thus $c_{\xi\xi k,i}$ will be very large at the node value i corresponding to $x = 0.2$. Therefore, the boundedness problem will arise during the initial time steps. Later, because of turbulent diffusion, the mixture-fraction gradients decrease and finally reach zero when the scalars are fully mixed. Thus, the final term in Eq. A3 will be insignificant for $0 \ll t$.

Observing the final term in Eq. A3, for small t the numerator is always nonnegative and very large near $x = 0.2$. In addition, because of the ICs, the denominator $(\langle\xi\rangle_{2,i}^{t} - \langle\xi\rangle_{1,i}^{t})$ will be proportional to ε where $0 < \varepsilon \ll 1$. Thus, for $t = 0$, the final term on the right-hand side of Eq. A3 will be dominant:

$$\langle\xi\rangle_{k,i}^{\Delta t} - \langle\xi\rangle_{k,i}^{0} \approx (-1)^k \frac{c_{\xi\xi1,i}^{0} + c_{\xi\xi2,i}^{0}}{\langle\xi\rangle_{2,i}^{0} - \langle\xi\rangle_{1,i}^{0}}\Delta t \qquad \text{for } k = 1, 2 \quad \text{(A5)}$$

If $1 - \varepsilon = \langle\xi\rangle_{2,i}^{0} \le \langle\xi\rangle_{1,i}^{0} = 1$, the right-hand side of this expression with $k = 1$ will be positive, and $\langle\xi\rangle_{1,i}$ will go out of bounds (that is, become greater than unity). Similarly, if $0 = \langle\xi\rangle_{1,i} \le \langle\xi\rangle_{2,i} = \varepsilon$, $\langle\xi\rangle_{1,i}$ will become negative. On the other hand, if $1 - \varepsilon = \langle\xi\rangle_{1,i}^{0} < \langle\xi\rangle_{2,i}^{0} = 1$, the right-hand side with $k = 2$ will be positive, and $\langle\xi\rangle_{2,i}$ will become greater than unity. Similarly, if $0 = \langle\xi\rangle_{2,i} \le \langle\xi\rangle_{1,i} = \varepsilon$, $\langle\xi\rangle_{2,i}$ will become negative. Thus, in either case (that is, $\langle\xi\rangle_{2,i}^{0} \le \langle\xi\rangle_{1,i}^{0}$ or $\langle\xi\rangle_{1,i}^{0} \le \langle\xi\rangle_{2,i}^{0}$), one of the mixture fractions will become unrealizable on the first time step.

In the absence of micromixing, the transported PDF model will predict that the mixture fraction in each notional particle remains at its initial value. Thus, for large t, 10% of the particles will have $\xi = 1$ and the other 90% will have $\xi = 0$. In the multienvironment PDF model, this condition would correspond to two delta functions, one with $p_1 = 0.1$ and $\langle\xi\rangle_1 = 1$, and the other with $p_1 = 0.9$ and $\langle\xi\rangle_1 = 0$. For the second ICs in Table 13, we can note that this condition will not be attainable using DQMOM-IEM(2), given that $p_1 = p_2 = 0.5$. However, the results above will hold for all initial values of p_k, and thus the boundedness problem will subsist even when $p_1 = 0.1$ and $p_2 = 0.9$ are used as the ICs. In fact, we have found that the boundedness problem can be avoided only by choosing ICs such that $c_{\alpha\alpha k,i}^{0} = 0$ for all scalars. This will occur only when the initial composition vectors $\langle\boldsymbol{\phi}\rangle_k(x, 0)$ are independent of x.

Note that the perturbation method given in Eq. A2 can lead to unrealizable results if the composition variables happen to lie on the boundary of the realizable domain. To handle this problem, in our numerical implementation, the DQMOM correction terms are added only when $\langle\xi\rangle_k \in [\varepsilon_1, 1 - \varepsilon_1]$, where ε_1 is a small positive number (such as 10^{-4}). Using this approach for the second ICs in Table 13, we have found that the predictions of the mixture-fraction variance are systematically smaller than those from the first ICs (which agree with the transported PDF results). On the other hand, if the realizability is not controlled, the mixture-fraction variance predictions for the second ICs match those from the first ICs. Thus, to check whether the results are affected by the realizability control algorithm for certain ICs, we can compare the results for the mixture-fraction variance with those obtained by not controlling for realizability.

Other numerical problems can arise and should be handled carefully in the numerical implementation. For example, p_k and $\langle\xi\rangle_k$ are bounded by 0 and 1, the reaction-progress variable Y and the moments m_i should be nonnegative. Our method to handle this issue is not to calculate correction terms when $\langle\boldsymbol{\phi}\rangle$ is close to its theoretical bounds, as illustrated for $\langle\xi\rangle$ in the previous paragraph. In the time-dependent code, decreasing Δt was also found to make the code more stable. This is most likely attributable to the explicit time-stepping algorithm, and further improvements would most likely result by using an implicit algorithm.

Finally, when the compositions in different environments are close to each other for a particular x location, the perturbation method can be applied. (This was found to occur at isolated points along the x-axis for every set of ICs investigated.) However, the perturbation value ε should be chosen carefully so that it does not cause scalars to go out of bounds. For example, different values of ε can be specified, and the results compared to make sure they are independent of the chosen value. Another approach to handle nondistinct compositions at a particular x location is to use the average correction terms from adjacent grid points (that is, $x + \Delta x$ and $x - \Delta x$).

Manuscript received Jul. 31, 2003, and revision received Dec. 1, 2003.